REPORT DOCUMENTATION PAGE

Form Approved
OMB No. 0704-0188

1. REPORT DATE *(DD-MM-YYYY)*	2. REPORT TYPE	3. DATES COVERED *(From - To)*
21-09-2005	Final Technical	4/1/2000 - 12/31/2004

4. TITLE AND SUBTITLE
Retrieval and Assimilation of Storm Characteristics from Both In-Cloud and Cloud-to-Ground Lightning Data to Improve Mesoscale Model Forecasts

5a. CONTRACT NUMBER

5b. GRANT NUMBER
N00014-00-1-0525

5c. PROGRAM ELEMENT NUMBER

6. AUTHOR(S)
Donald R. MacGorman

5d. PROJECT NUMBER

5e. TASK NUMBER

5f. WORK UNIT NUMBER

7. PERFORMING ORGANIZATION NAME(S) AND ADDRESS(ES)
University of Oklahoma
Norman, OK

8. PERFORMING ORGANIZATION REPORT NUMBER

9. SPONSORING/MONITORING AGENCY NAME(S) AND ADDRESS(ES)
Office of Naval Research Regional Office San Diego
4520 Executive Drive, Suite 300, San Diego, CA 92121-3019

10. SPONSOR/MONITOR'S ACRONYM(S)
ONR

11. SPONSOR/MONITOR'S REPORT NUMBER(S)

12. DISTRIBUTION/AVAILABILITY STATEMENT

DISTRIBUTION STATEMENT A
Approved for Public Release
Distribution Unlimited

13. SUPPLEMENTARY NOTES

14. ABSTRACT
To improve the accuracy of regional weather forecasts, we (1) obtained and operated a lightning mapping system that detects all types of lightning to provide data for this project, (2) quantified and tested relationships between lightning and other storm properties that will be useful for assimilation, and (3) developed techniques for assimilating data from all types of lightning into COAMPS. Observational data analysis and storm simulations showed that total lightning flash rates were correlated with a storm's mass and volume of graupel, updraft mass flux through the mixed phase region, and the volume of updraft exceeding 10 m/s. Gridded lightning data were assimilated into COAMPS by nudging the trigger function of the Kain-Fritsch subgrid-scale convective parameterization. In a test case from the central United States in July 2000, assimilation of lightning data greatly improved the surface moisture, the intensity and location of surface cold pools, and the location of deep convection at the time of forecast initialization. The best results were obtained when convection was completely suppressed where no lightning was observed.

15. SUBJECT TERMS
Lightning, data assimilation, weather forecast, COAMPS, correlation, mesoscale model, thunderstorm, graupel, updraft

16. SECURITY CLASSIFICATION OF:			17. LIMITATION OF ABSTRACT	18. NUMBER OF PAGES	19a. NAME OF RESPONSIBLE PERSON
a. REPORT	b. ABSTRACT	c. THIS PAGE		57	Jennie I. Parker, Sponsored Programs Coordinator
					19b. TELEPHONE NUMBER *(Include area code)* (405) 325-6054

Final Report to the Office of Naval Research
ONR Grant # N00014-00-1-0525

Retrieval and Assimilation of Storm Characteristics from Both In-Cloud and Cloud-to-Ground Lightning Data to Improve Mesoscale Model Forecasts

Donald R. MacGorman[1,2,3], Conrad L. Ziegler[3], Edward R. Mansell[1],
William H. Beasley[2], and Brian H. Fiedler[2]

[1]CIMMS/University of Oklahoma, Norman
[2]School of Meteorology/University of Oklahoma, Norman
[3]NOAA/National Severe Storms Laboratory, Norman, OK

September 2005

EXECUTIVE SUMMARY:

To improve the accuracy of regional weather forecasts, the following were accomplished: (1) obtained, installed, and operated a lightning mapping system that detects all types of lightning to provide data for this project; (2) quantified and tested relationships between lightning and other storm properties that will be useful for assimilation; (3) developed techniques for assimilating data from all types of lightning into the COAMPS mesoscale forecast model.

To provide lightning data for this project, the University of Oklahoma Regents purchased a three-dimensional VHF lightning mapping system, the Lightning Mapping Array (LMA), which was installed in central Oklahoma in cooperation with the National Severe Storms Laboratory. Because a fire destroyed the initial system, installation was delayed 15 months. Therefore, we also used data from a similar system that had recently been deployed in Kansas for the STEPS field program.

Analysis of a few case studies and storm simulations of many cases showed that total lightning flash rates were correlated with the mass and volume of graupel in a storm, with the updraft mass flux through the mixed phase region, and with the volume of updraft exceeding 10 m s^{-1}. Correlations were also found with parameters related to the potential for hail and tornadoes. Similar relationships are being analyzed for many more cases with data from the central Oklahoma LMA.

Techniques were developed for continuously assimilating ground strike and total lightning data into the COAMPS mesoscale forecast model, to improve initial conditions for the forecast period. Data were assimilated by using the trigger function of the Kain-Fritsch subgrid convective parameterization. Where lightning was observed, moisture was nudged in 0.1 g kg^{-1} increments (to a maximum of 1 g kg^{-1}) until a parcel in the most unstable layer ascended to an altitude $\geq$7 km and achieved an updraft speed of 10 m s^{-1}. Options were added to weaken or eliminate convection in a grid cell if lightning was not observed there.

In a test case from the central United States in July 2000, assimilation of lightning data greatly improved soil moisture, quantitative precipitation estimates, the location and intensity of surface cold pools, and the location of deep convection at the time of forecast initialization. The best results were obtained when convection was completely suppressed where no lightning was observed. Improving initialization was the main goal of our assimilation, but effects on the forecast also were studied. The location and amounts of model precipitation diverged increasingly from observations during the forecast period, but up to twelve hours later showed some improvement over the forecast based on no assimilation. It appears that the increasing discrepancy with time was caused at least partly by the tendency of COAMPS to produce too little subgrid-scale convective precipitation. Even during the assimilation cycle, the larger rainfall rates were 40% of observed rates, and this decreased to 20% of observed rates in the first hour of the forecast. Similarly, the forecast temperature gradients weakened with time, whereas observed temperature gradients remained strong. Our hypothesis is that the under-production of subgrid-scale rainfall also reduced surface cooling and outflow boundaries, which tended to weaken subsequent triggering of convection; this, in turn, subsequently produced an even greater shortage of subgrid and resolvable scale rainfall in a feedback cycle.

Though this project was successful (a) in developing techniques for assimilating total lightning data and (b) in finding relationships between lightning and other storm properties that may be useful for assimilation, several issues remain: (1) Broaden the analysis of relationships between lightning other storm properties to many more cases, to provide a better statistical basis for assimilation. (2) Find ways to reduce the under-production of subgrid-scale convective precipitation in COAMPS so that improvements will extend farther into the forecast period. (3) Develop assimilation techniques that use lightning not only to turn the convective trigger function on or off, but also to influence the strength and character of the convection.

ABBREVIATIONS

AGL	above ground level
BL	boundary layer
BRN	Bulk Richardson Number
BWER	bounded weak echo region
CAPE	convective available potential energy
CBL	convective boundary layer
+CG	positive cloud-to-ground
CG	cloud-to-ground
CIN	convective inhibition
CL	confidence level
CONUS	continental United States
CPS	convective parameterization scheme
EFM	electric field meter
EL	equilibrium level
ERL	elevated residual layer
fC	10^{-15} Coulombs
GZ	Gardiner-Ziegler noninductive charging scheme
IC	in-cloud or intracloud
KF	Kain-Fritsch subgrid-scale convective parameterization scheme
LCL	lifting condensation level
LFC	level of free convection
LMA	Lightning Mapping Array
MCS	mesoscale convective system
MEaPRS	MCS Electrification and Precipitation Radar Study
MSL	mean sea level
MVOI	multivariate optimal interpolation
NCAR	National Center for Atmospheric Research
NCEP	National Centers for Environmental Prediction
NLDN	National Lightning Detection Network
NMIMT	New Mexico Institute of Mining and Technology
NSF	National Science Foundation
NSSL	National Severe Storms Laboratory
OK-LMA	Oklahoma Lightning Mapping Array
ONR	Office of Naval Research
OU	University of Oklahoma
QPE	quantitative precipitation estimate
QPF	quantitative precipitation forecast
RAR	rime accretion rate
RAR_{crit}	critical rime accretion rate value
RR	Riming Rate noninductive charging scheme
SP98	Saunders and Peck (1998) noninductive charging scheme
SRH	storm relative helicity
STEPS	Severe Thunderstorm Electrification and Precipitation Study
TAKA	Takahashi noninductive charging scheme

UTC	Coordinated Universal Time
VCP	volume coverage pattern
VHF	Very High Frequency
VIL	vertically integrated liquid
WATADS	WSR-88D Algorithm Testing and Display System
WSR-88D	National Weather Service (1988 version) Doppler radar

TABLE OF CONTENTS

BACKGROUND AND GOALS OF THE STUDY

To improve the accuracy of regional weather forecasts, we proposed (1) to document relationships suitable for use to retrieve storm properties from satellite lightning data and (2) to develop techniques for assimilating information from lightning into numerical forecast models during model initialization. Lightning data have several advantages over radar data and cloud top imagery in depicting convection for assimilation into numerical forecast models. For example, lightning data are more compact and easier to handle for storm identification. Probably the most important advantage is that lightning flash data can be readily obtained for regions in which radar observations are sparse or completely unavailable, such as mountains and oceans.

Prior to our project, the few studies that had examined assimilation of lightning data used data only from flashes that struck ground (cloud-to-ground flashes, i.e., ground flashes), largely because data sets that included all types of lightning were not available over a large enough region or for a long enough time to be useful for assimilation. However, using data from all types of lightning is desirable for several reasons: (1) Lightning that does not strike ground (cloud flashes) and cloud-to-ground lightning are related to different processes of a storm and so provide complementary information. Cloud flash rates are related to the magnitude of the updraft and the mass or volume of precipitating ice in the mixed phase region, while cloud-to-ground flash rates are related more to the formation of precipitation at middle to lower levels of a storm (e.g., Goodman et al. 1988, MacGorman et al. 1989; Williams et al. 1989). (2) Systems that map both types of lightning detect thunderstorms more reliably, because there are more events to detect. Almost all flashes in many storms are cloud flashes, and overall there are 2-3 times as many cloud flashes as cloud-to-ground flashes (e.g., pages 190-192 and 229-234 of MacGorman and Rust 1998). Furthermore, the first few flashes in a storm usually are cloud flashes, so using cloud flash data improves the timeliness of storm identification. (3) Satellite lightning mapping systems provide the most practical and secure means for mapping thunderstorms globally, and such systems detect both types of lightning. Lightning sensors have already been deployed in various low Earth orbits. Deployment in a geostationary orbit is technically feasible at a reasonable cost.

To begin using total lightning data for numerical weather forecast models, we proposed several tasks: (1) Obtain and operate a lightning mapping system that detects both cloud and cloud-to-ground lightning to provide data sets for all aspects of this project. (2) Quantify and test relationships between lightning and other storm properties for use in assimilation routines. (3) Develop techniques for assimilating data from all types of lightning into numerical mesoscale forecast models, particularly COAMPS. (4) Evaluate how limitations imposed by the operational characteristics of satellite sensors affect the performance of various lightning assimilation techniques.

Because our funding was reduced from the requested level, plans to address the initially proposed tasks were reduced somewhat. The fourth goal was eliminated entirely. However, a subsequent study by another research group (Thomas et al. 2000) provided at least an initial examination of this issue. They found, as one might expect, that an optical satellite mapper responds best to lightning in the upper half of the cloud and responds poorly to lightning in the lower part of clouds or below cloud base. We expect that, in most storms, this detection behavior will have little or no negative effect, because a storm's initial lightning flashes typically occur high enough to be detected readily. However, there may be occasional exceptions in which lightning activity begins lower in the cloud, so storm detection may occasionally be delayed a few minutes when using an optical satellite lightning mapper.

RESULTS

Task 1. Obtain and operate a lightning mapping system that detects all types of lightning:

A system that maps all lightning reliably over large distances was needed both for the storm analysis and data assimilation tasks of our grant. To address this task, matching funds were provided by the University of Oklahoma Regents to purchase a VHF Lightning Mapping Array (LMA) developed by New Mexico Institute of Mining and Technology (NMIMT). The system was delivered initially in late June 2001, but within a few days, fire completely destroyed the warehouse in which the equipment was temporarily stored. Funds to purchase a replacement were provided by insurance and by the University of Oklahoma. The replacement system was delivered in August 2002, and installation in central Oklahoma was completed by November 2002. (Figure 1 shows the present configuration). Though operation began then, the storms needed to test data acquisition did not occur until December. Data have been archived continually for this project since winter 2003. Figure 2 shows an example of storms mapped by the system.

For maintaining the system and testing operational applications, it was desirable to map lightning in real time, though this was not required for the present project. The system had been designed so that data could be sent via radio to a central processor that controlled the network. In winter 2004, software to handle the real-time processing were implemented, and the system began producing real-time lightning locations. It has provided real-time data continually since then. The real-time data are being provided to experimental weather operations for the first time in 2005. Real-

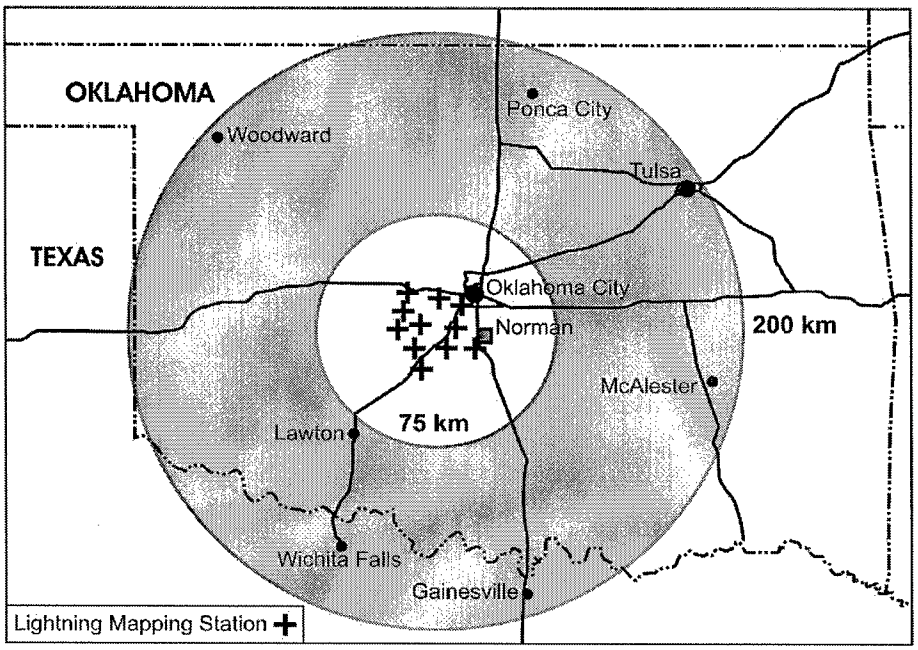

Figure 1. Map of the Oklahoma Lightning Mapping Array. The inner circle indicates the range of three-dimensional lightning mapping coverage. The outer circle indicates the nominal range of two-dimensional lightning mapping coverage. The control center is in Norman.

time data make possible a quasi-operational test of lightning data assimilation into a numerical weather forecast model, but this is beyond the scope of the proposed work and has not yet been done.

Because installation of the Oklahoma LMA (OK-LMA) was delayed so long, we worked with colleagues to obtain some lightning mapping data sets from existing networks elsewhere to get started on this project. The data sets on which we concentrated our analysis were obtained from systems almost identical the OK-LMA, operated by New Mexico Institute of Mining and Technology during field programs in which we collaborated for three weeks in 1998 (the MCS Electrification and Precipitation Radar Study or MEaPRS) and for seven weeks in 2000 (the Severe Thunderstorm Electrification and Precipitation Study or STEPS).

Data from the OK-LMA were used in a major field program funded by the National Science Foundation (NSF) in 2003 and 2004. Considerable observational resources were added to the OK-LMA, including a polarimetric radar, two mobile Doppler radars, environmental soundings, and electric field soundings. These data will enable further progress addressing both the second and third

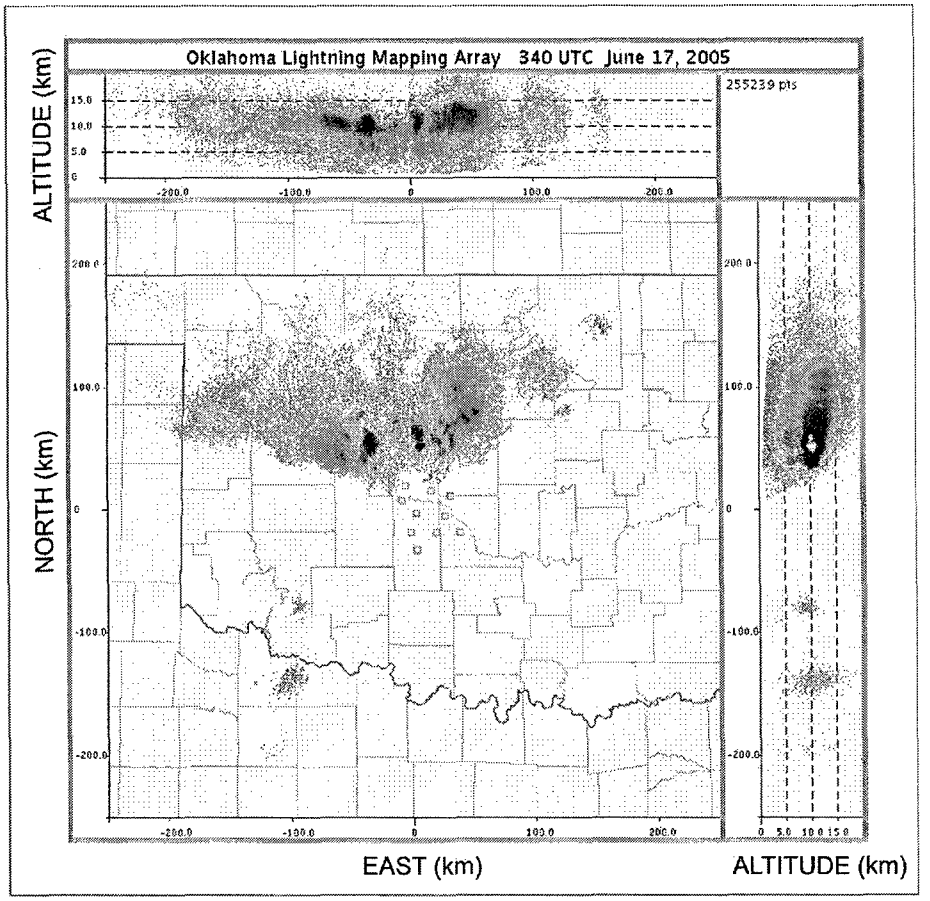

Figure 2. Lightning mapped in real time by the Oklahoma Lightning Mapping Array for a squall line at 0340-0350 UTC on 17 June 2005. Shading color indicates the number of mapped channel segments per square kilometer, with violet indicating the smallest densities and white indicating the largest densities. (Real-time figure is courtesy of New Mexico Institute of Mining and Technology.)

tasks in future years. Though we do not yet have funding to continue the data assimilation research, some observational studies of relationships between lightning and other storm properties that are relevant to the present project are being funded by NSF and will continue for the next 2-3 years. Furthermore, OK-LMA data are being used to develop new real-time products for experimental operations at the National Weather Service to explore ways in which the lightning data can be used by forecasters to improve diagnosis and warning of storm hazards. Thus, ONR's investment in this project is being leveraged to continue work of benefit to ONR.

Task 2. Quantify and test relationships between lightning and other storm properties for use in assimilation routines:

Our initial assimilation techniques, developed under this proposal and described under Task 3, used lightning data simply to provide the location and timing of thunderstorms. However, one longer term goal is to develop techniques that use lightning data to influence the character of the subgrid-scale convection, not just its occurrence. To begin providing the information about relationships between lightning and storms needed for this application, we developed a three-pronged approach: (1) a case study of one storm to examine the relationship of lightning rates and distribution with ice mass inferred from polarimetric radar and with vertical storm development, (2) a statistical study of the relationship of lightning flash rates with various radar-derived storm characteristics for several storms, and (3) a numerical storm simulation of an observed storm to provide complete model fields of major storm properties for comparison with lightning flash trends.

2.1. Case Study of a Storm

The MCS Electrification and Polarimetric Radar Studies (MEaPRS) field program was based in central Oklahoma in 1998. Data acquired by MEaPRS included data from a 10-cm polarimetric radar operated by the National Severe Storms Laboratory (NSSL) and from the prototype lightning mapping array operated by New Mexico Institute of Mining and Technology (NMIMT) (Krehbiel et al. 2000, Rison et al. 1999, Thomas et al. 2004). Coverage by the New Mexico system was similar to coverage of the Oklahoma lightning mapping array in Fig. 1, but was shifted roughly 50 km NNW. One of the storms observed by MEaPRS was a supercell storm that produced weak to strong tornadoes in the Oklahoma City area on June 13. This storm was positioned well for data collection by both the lightning mapping array and the polarimetric radar for roughly one hour, during which it produced tornadoes and large hail.

As shown in Fig. 3, total flash rates exceeded 100 per minute throughout almost the entire analysis period. Most flashes were cloud flashes. Cloud-to-ground flash rates were typically ≤ 2 per minute, but tended to be larger during the two F-2 tornadoes, the maximum rate being 7 per minute. Approximately 90% of all cloud-to-ground flashes that occurred during the analysis period were the anomalous flashes that lower positive charge to ground, instead of the usual negative charge. Also, many of the cloud flashes that occurred in the upper part of the storm during this period appeared to discharge negative charge above positive charge, a vertical polarity inverted from what is normally observed. Shortly after the storm moved beyond the range of three-dimensional lightning mapping data (after the period shown here), it weakened and dissipated, and most subsequent cloud-to-ground lightning lowered negative charge to ground. All tornadoes ended before the change in dominant ground flash polarity.

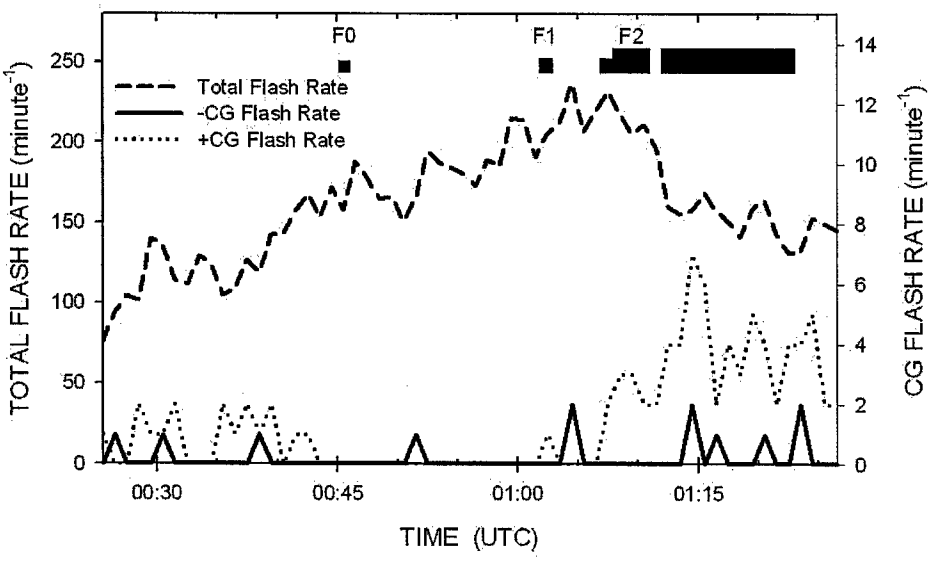

Figure 3. Flash rates from the tornadic supercell storm that occurred in central Oklahoma on 13-14 June 1998. Only those flashes having at least 10 mapped points were tabulated in the total flash count. The time of each tornado that occurred during this period is indicated by a black bar whose height indicates the tornado's F-scale rating. (The F scale ranges from F0 to F5, weak to violent. F2 is considered strong.)

Figure 4 shows that trends in the number of VHF radiation sources from lightning at 8–10 km MSL were similar to trends for the mass of graupel near and within the mixed phase region of the storm. The hydrometeor properties shown in the figure were inferred from polarimetric radar data by using the algorithms of Lopez and Aubagnac (1997). Laboratory studies (e.g., Takahashi 1978, Jayaratne et al. 1983, Saunders et al. 2001) and an increasing body of storm observations (e.g., Dye et al. 1986, Bringi et al. 1997, Black and Hallett 1999) have suggested that storm electrification is caused by noninductive charge exchange during rebounding collisions of actively riming graupel and cloud ice. The relationship between graupel mass and number of VHF sources provides further support to the hypothesis that the noninductive graupel-ice mechanism is responsible for much of storm electrification.

The relative minimum in both VHF lightning radiation source rates and graupel mass between 0055 and 0100 UTC overlapped and followed a period in which the mass of hail increased at middle levels. It appears likely that hail grew at the expense of graupel during this period. Furthermore, the smallest VHF source rates during this period corresponded to an increase in the mass of wet hail at temperatures colder than freezing. This increase suggests that updrafts became strong enough to cause wet growth of precipitating ice in some regions. Wet growth would contribute essentially nothing to electrification by the noninductive graupel-ice mechanism, because when colliding ice particles become wet, rebounding tends to cease.

Some information about updrafts may be inferred from the vertical development of lightning activity (Fig. 4). Between approximately 0040 and 0115 UTC, over-shooting turrets of lightning activity appeared at roughly 10-minute intervals. The upward slant with time in each turret is suggestive of a rising surge in the updraft. For some of the turrets, it is possible to extrapolate the slant downward in space and backward in time to periods of increasing VHF sources at lower

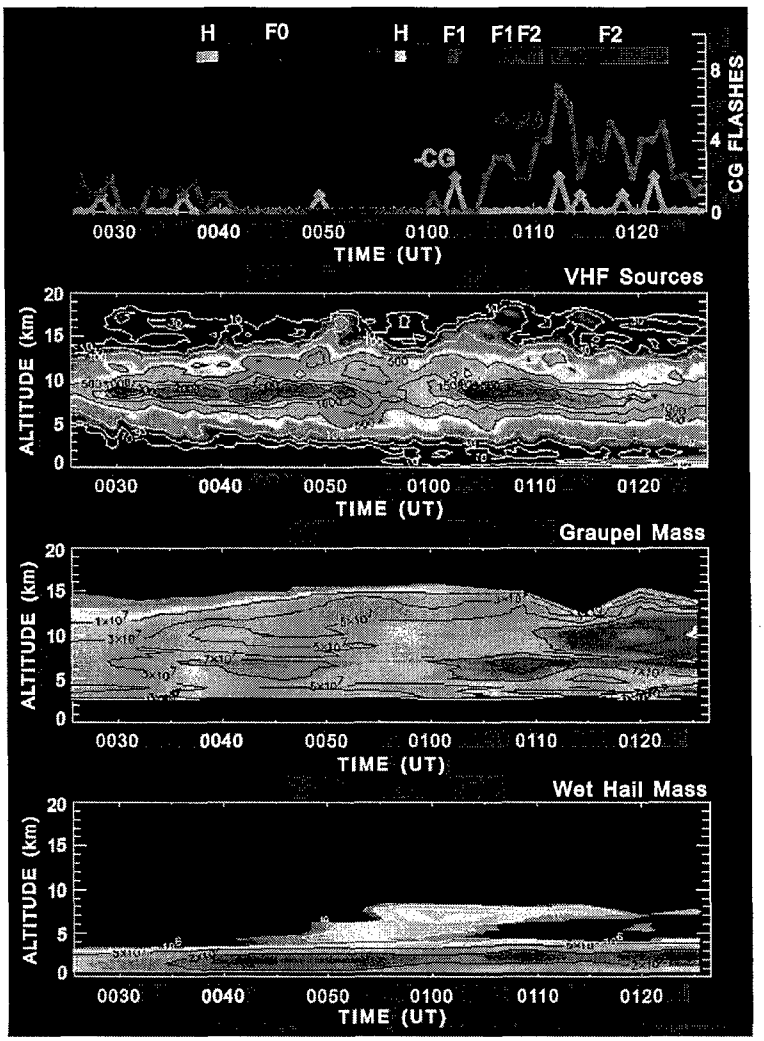

Figure 4. Cloud-to-ground (CG) lightning flash rates with time-height plots of lightning channel segments mapped by the VHF system and of graupel mass and wet hail mass inferred from the NSSL polarimeteric S-band Doppler radar (a modified WSR-88D) for the tornadic supercell storm on 13 June 1998. The time-height plot of lightning shows the sum of all the VHF sources in each 0.5-km horizontal slice each minute. The time-height plots of inferred particle mass summed the mass in the same 0.5-km slices for each radar volume scan.

altitudes. The beginning of the highest-reaching and most sustained turret (note the increasing number of VHF sources apparent at ≥ 14 km MSL beginning at roughly 0100 UTC) appears to correspond to the earlier rapid increase in mass of wet hail at middle levels (Fig. 4). The number of VHF sources at 8–10 km MSL had a relative minimum at the beginning of this period, but soon began increasing. It reached its maximum value for the entire analysis period at 0105–0109 UTC.

It appears from these data that this extremely strong updraft surge led to wet growth of graupel and hail beginning at roughly 0055 UTC. As ice particle growth becomes wet, ice density increases (becoming more hail-like), particle collection efficiency increases, and ice-particle collisions are much less likely to rebound. We would expect these effects to be sufficient to cause the observed decrease in graupel mass and electrification as the updraft intensified. However, graupel mass (and lightning activity) soon began increasing again, probably a result of increases in both the size and number concentration of graupel, as wet growth subsided when the strong, sustained updraft surge weakened somewhat, though remaining strong.

A combination of the above microphysical and kinematic inferences may provide some insight into the cause of the larger positive cloud-to-ground flash rates between 0105 and 0125 UTC in Fig. 4. Though it appears that the large updraft surge led to wet growth in at least some regions, we hypothesize that, in somewhat weaker regions of the updraft, graupel was not in wet growth, though the liquid water content was larger than usual. Essentially all modern laboratory studies of noninductive charging (e.g., Takahashi et al. 1978, Jayaratne et al. 1983) indicate that actively riming

graupel gains positive charge, instead of the more usual negative charge, during rebounding collisions with cloud ice when the liquid water content is unusually large (but not large enough to cause wet growth). If such a reversal were sustained enough, it would cause a corresponding reversal of at least part of the charge distribution of the storm itself. Such a reversal would replace the negative charge normally tapped by cloud-to-ground flashes with positive charge.

Our hypothesis, therefore, is that the strong updraft surge on June 13 eventually led to an increase in cloud-to-ground flash rates, but that unusually large liquid water contents in the mixed phase region led to a reversal in the polarity of the charge distribution. This reversal, in turn, reversed the polarity of cloud-to-ground flashes. Note that Rust and MacGorman (2002) presented evidence that the polarity of the charge distribution is inverted from normal in some, but not all, storms that produce positive cloud-to-ground lightning. Thus, this hypothesis may explain some, but probably not all, occurrences of positive cloud-to-ground lightning.

Trends in lightning activity and tornado occurrence were consistent with the hypothesis that increases in lightning activity due to large updraft surges tend to lead severe weather occurrence. However, increases in flash rates were neither as prominent nor as clearly associated with severe weather as those reported for Florida severe storms by other investigators (e.g., Williams et al. 1999), possibly because flash rates were very large throughout most of the period of the Oklahoma City storm. In this storm, the rate of VHF emissions tended to increase at middle levels of the storm prior to tornadoes. Tornadoes tended to occur during or shortly after the updraft surges inferred from lightning, consistent with hypotheses and limited observations by other scientists suggesting that strong tornadoes tend to occur as updraft surges weaken. In particular, the two most violent tornadoes began during the latter stages of, or just after, what appeared to be the dissipation of the largest, most sustained updraft surge.

2.2. Statistical Study of Lightning and Radar-inferred Storm Properties

2.2.1. Sources of Data

The data used in this study were collected by the Severe Thunderstorm Electrification and Precipitation Study (STEPS). The STEPS field program took place in May - July 2000 in Kansas, Colorado, and Nebraska, to collect comprehensive data sets from severe storms over the High Plains of the United States (Lang et al. 2004). One of the main goals of the project was to achieve a better understanding of the interactions among storm kinematics, microphysics, electrification, and lightning. Numerous storms, including supercells, short-lived multicell storms, and large mesoscale convective complexes, were documented during STEPS.

STEPS instrumentation included two polarimetric Doppler radars, a National Weather Service (1988 version) Doppler radar, an instrumented aircraft, a mobile ballooning team to provide in situ electric field and thermodynamic soundings of storms, the National Lightning Detection Network (NLDN) (Cummins et al. 1998), and a three-dimensional VHF Lightning Mapping Array (LMA) deployed by the New Mexico Institute of Mining and Technology (NMIMT) (e.g., Rison et al. 1999). The NLDN determines the time, latitude, and longitude at which a lightning flash struck ground and estimates the magnitude and polarity of the peak return-stroke current. The LMA determines the latitude, longitude, altitude of the source of the signal, the reduced chi-squared statistic of the estimated VHF source location, the radiated power, and the number of stations that recorded the signal of the mapped VHF source. The LMA can map a flash in 3-D within roughly 75 km of the center of the array. A map of the LMA during the STEPS field program is shown in Fig. 5.

Points mapped by the system were grouped into flashes by using temporal and spatial criteria. For a new point to be added to an existing flash, it had to occur within 0.15 s and 3 km of any of the

previous points in the flash. If two or more flashes were identified as ongoing at the same time, the algorithm tested whether to merge the individual flashes into one each time a point was added to one of them, because many of the initially identified flashes actually may have been branches of one larger flash. One of the other flashes was merged with the flash to which a point had just been added if (1) the added point was within 0.3 second of any point in the other flash and (2) any point in one flash was within 3 km of any point in the other flash. However, if merging the two flashes would create a flash duration 4 s or longer, the flashes were not merged, but kept separate. No flash was allowed to exceed 4 s in duration, but this limit was rarely, if ever, reached.

Once a flash was considered finished (i.e., new points were more than 0.3 s after the last point in the flash), it then was sorted into a category according to the number of mapped points it included: extra small flashes had <11 points per flash, small flashes had 11-44 points per flash, medium flashes

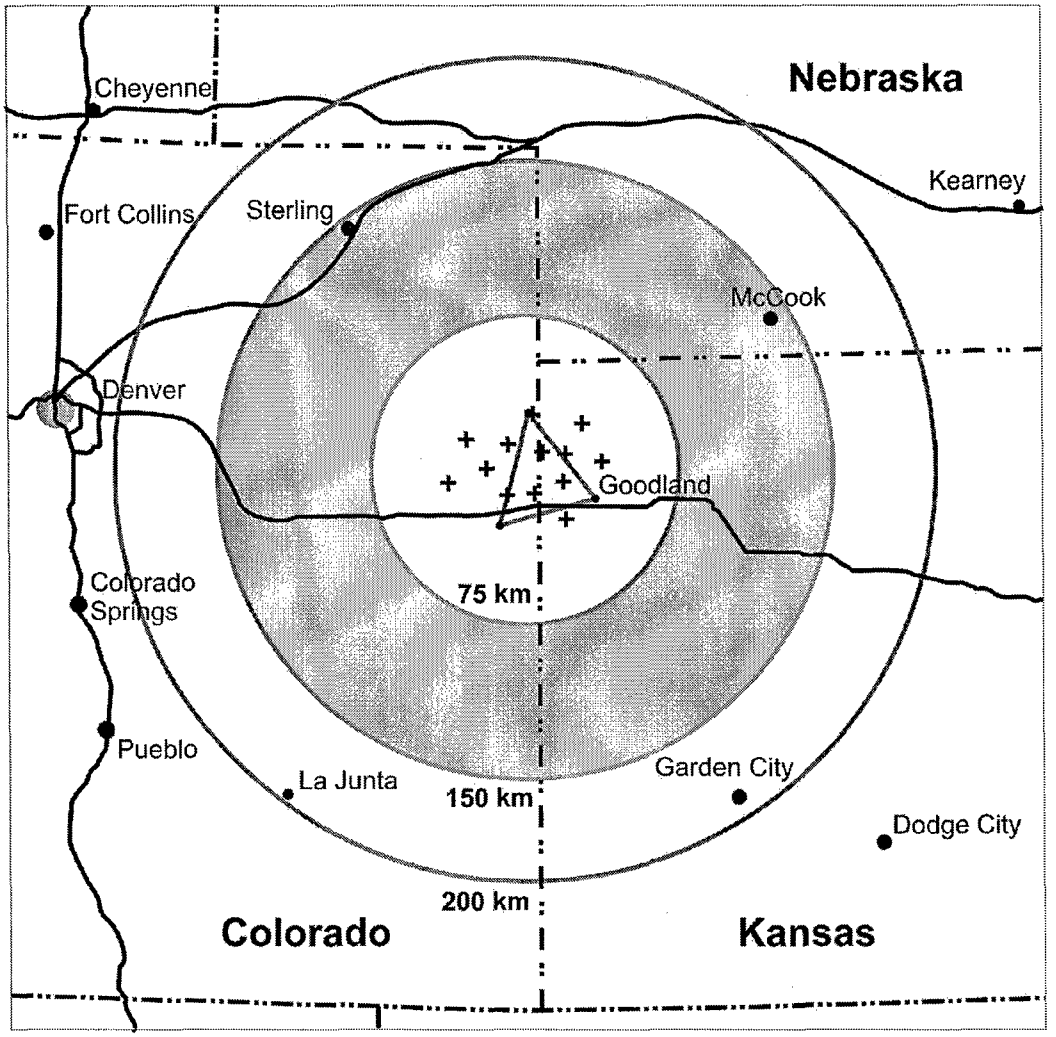

Figure 5. Map of the location of three radars (vertices of the triangle) and stations in the Lightning Mapping Array (pluses) during STEPS in summer 2000. The inner circle was the primary STEPS operational area, with three-dimensional lightning mapping coverage. The 150-km circle was the maximum range of STEPS operations; 200 km is the nominal range of the LMA.

had 45-1192 points per flash, large flashes had 1192-6181 points per flash, and extra large flashes had >6181 points per flash. The boundaries of these size categories were determined by transforming the distribution of flash sizes to a distribution that was roughly Gaussian and then defining the sizes within one standard deviation of the mean as medium, sizes between one and two standard deviations as either small or large, and sizes more than two standard deviations from the mean as extra small or extra large. Extra small flashes were omitted from most of the subsequent analyses, because one-point flashes dominated the category and many of these were due to noise, not lightning. With extra-small flashes omitted, trends in total flash rates and in the flash rates of each of the other categories were analyzed relative to trends in storm characteristics inferred from radar and observers.

The radar used in this study was the WSR-88D radar at the Weather Service Forecast Office in Goodland, Kansas (the easternmost radar in Fig. 5). The 10-cm wavelength radar collected data using volume coverage pattern (VCP) 11, described by Alberty et al. (1991). This operational mode completes a volume scan of 14 different elevation angles, from 0.5° to 19°, in 5 minutes.

Since the correlation between radar parameters and lightning is the focus of this study, only storms that were within both the WSR-88D radar range and within the LMA's three-dimensional coverage were considered. Out of 19 storm days, six cases were selected: 3 June 2000 (called Bird City in figures and tables), 11 June 2000 (Idalia 1), two cases from 22 June 2000 (Burlington and Idalia 2), 24 June 2000 (Haigler), and 29 June 2000 (Wheeler).

The radar-inferred storm cell parameters were determined by the WSR-88D Algorithm Testing and Display System (WATADS) (see WATADS 2000). The cell parameters used in this study were vertically integrated liquid (VIL) in kilograms of water per meter squared (kg/m^2), height of 30 dBZ reflectivity (height) in kilometers, estimated hail diameter (hail diam.) in millimeters, percent probability of hail of any size (%hail), percent probability of severe hail (diameter > 0.75 in) (%SVRH), and the type of rotation detected (weak circulation, mesocyclone, or tornado vortex signature). Other storm parameters were determined manually: the total number of cells within the 45 dBZ base reflectivity contour (number of cells in 45 dBZ), the horizontal area of the 45 dBZ base reflectivity contour (area of 45 dBZ contour), and the maximum number of cells that would fit within a 10 km radius of any given cell in the 45 dBZ base reflectivity contour (number of cells in 10 km). Hail and tornado reports were obtained from *Storm Data*.

The storm parameters for this study were collected from the strongest cell (determined by VIL, rotation signature, and hail probabilities) in each five-minute volume scan of the storm. The strongest cell was chosen as representative of the storm. Though it is possible to correlate the time series for individual cells, our goal was to characterize relationships for the storm overall. Since cells within a storm grow and dissipate within the storm's lifetime, it was usually the case that, as one cell dissipated another cell in the same vicinity became the strongest cell, so the parameter values were then taken from that cell.

To match the lightning flash counts with radar parameters in time, lightning flash counts were tabulated over the same 5-minute periods spanned by the radar volume scans. For large storm systems, only the part of the storm within the range of three-dimensional lightning mapping was used for both the radar and lightning analyses. Mapped lightning points from other storms and from outside the three-dimensional coverage of the LMA were eliminated before sorting the points into flashes, as described above.

2.2.2. Correlation Analysis Technique

To compare the timing and strength of correlations between lightning and storm parameters, the flash counts of CG flashes and of all flashes detected by the LMA were cross-correlated with the

storm parameters determined from radar analyses and observers. These correlations were calculated by using Pearson's Correlation Coefficient (Wilks 1995)

$$r = C_{xy} / S_x S_y , \qquad \text{Equation 3.1}$$

where C_{xy} is the covariance, S_x is the standard deviation for the x variable and S_y is the standard deviation of the y variable. Tests of statistical significance were performed to determine how likely the correlation coefficients were to be obtained by chance. The statistic used for the t-test is:

$$t = r\sqrt{[(n-2)/(1-r^2)]} , \qquad \text{Equation 3.2}$$

where n is the number of observations.

Since the samples of data in adjacent 5-minute periods are typically not independent, the decorrelation time of the variables had to be obtained before calculating the critical t-value. This was done by correlating the last n-1 data points (e.g. 2-100) with the first n-1 (1-99) data points until the correlation coefficient was zero (or close to zero). The decorrelation time, τ, is the number of steps it took for the correlation to become zero. An Effective Degrees of Freedom (Edf) is obtained for each variable by:

$$Edf = n/\tau \qquad \text{Equation 3.3}$$

The critical Degrees of Freedom (DF_c) is then simply the average of the two Effective Degrees of Freedom and is thus obtained by:

$$DF_c = (Edf_1 + Edf_2)/2 \qquad \text{Equation 3.4}$$

where Edf_1 is the Effective Degrees of Freedom for the first variable and Edf_2 is the Effective Degree of Freedom for the second variable. The critical t-value (t_c) is then found from a standard Student's t-distributions table by using the critical degrees of freedom. Fractional values of the degrees of freedom were rounded to the nearest integer, and the critical t-value was obtained by using the integer value. Correlation coefficients are significant if the t-value of the data is greater than the critical t-value for a certain confidence level (C.L). The 90%, 95% and 99% C.L. were used in the present study.

Because the cycle of any storm process related to lightning might be shifted in phase from the cycles of flash rates, the correlation analysis considered offsets in time between pairs of parameters from -15 minutes to +15 minutes, in 5-minute steps. A positive offset meant the radar parameter led the lightning flash rate; negative meant the flash cycle lagged the radar parameter cycle. The number of samples that were used in the correlation computation had to be reduced by one for each 5 minutes of lag or lead that was introduced. For example, an offset of +5 minutes in a storm which was sampled 30 times over a period of 150 minutes meant that samples 1-29 of the radar data were correlated with samples 2-30 of flash rates.

2.2.3 Correlation Results

The storms included in this analysis varied widely. Storms were small and isolated on 3 June and were a complex group of cells on 24 June. A tornadic supercell storm occurred on 29 June, and a weak tornadic storm was the first storm analyzed on 22 June. On 11 June and later on 22 June,

multicellular storms interacted to form small mesoscale convective systems.

Lightning characteristics in these storms varied considerably. Some of these characteristics are summarized in Table 1. Note that all of the storms that had cloud-to-ground lightning produced mostly ground flashes that lowered positive charge to ground, instead of the usual negative charge. Furthermore, cloud-to-ground flashes comprised a more consistently small fraction of total lightning activity than is usually observed elsewhere. The storm with the smallest flash rates had no cloud-to-ground flashes at all, though its maximum cloud flash rate was still fairly large.

The results of correlating the radar-inferred parameters with flash rates for all lightning in the small category or bigger are shown in Table 2. Note that almost all analyzed radar-inferred storm parameters are correlated with total lightning flash rates at a confidence level of 90% or better for every storm. Lightning flash rates appear to correlate reasonably well with all radar-inferred measures of storm strength.

However, flash rates were correlated better with some parameters than with others. The correlation coefficients were consistently highest for the area within 45 dBZ contours and either severe hail probability or hail probability. These two correlations were always significant at the 95% level or better. Except for the storm on 24 June, the three highest correlation coefficients for each storm were consistently greater than 70%. On 24 June, they were only 50-57%. The 24 June storm was a very complex storm, involving the interactions of multiple surface boundaries, with widely varying cell tracks that sometimes crossed.

In those storms that had cloud-to-ground flashes, (13 June did not), ground flash rates were correlated less well than cloud flash rates with the radar-inferred storm parameters, as shown in Table 3. In the 24 June storm, no radar-inferred parameter was correlated with either positive or negative

Table 1. Lightning flash characteristics for the six STEPS storms included in this study.

A

Average Flash Rates (per min)		
Storm	**CG**	**Total**
Bird City	0.00	8
Idalia 1	1.08	162
Idalia 2	3.06	237
Burlington	0.41	110
Haigler	0.88	127
Wheeler	0.69	65
AVERAGE	1.02	118

B

Maximum Flash Rates (per 5 min)		
Storm	**CG**	**Total**
Bird City	0	126
Idalia 1	14	1804
Idalia 2	44	2546
Burlington	9	490
Haigler	18	1026
Wheeler	16	571

C

Percent CG of Total Flashes	
Storm	**CG**
Bird City	0.0
Idalia 1	0.7
Idalia 2	1.3
Burlington	0.4
Haigler	0.7
Wheeler	1.1

D

Percent +CG of Total CG Flashes	
Storm	**CG**
Bird City	NA
Idalia 1	71
Idalia 2	67
Burlington	54
Haigler	52
Wheeler	87
Overall	66

Table 2. Largest correlations (in +/- 15 minutes) between radar-inferred parameters and total flashes. R_L is the correlation coefficient. Lag is the offset step having the largest correlation coefficient and is positive if the radar inferred parameter leads lightning, negative if the radar-inferred parameter lags. T, 90%, 95%, and 99% are, respectively, the data t-test value, the t-value of the 90% confidence level, of the 95% confidence level, and of the 99% confidence level. The correlation is significant at a particular level if the data's t-test value is larger than the t-value of the confidence level. The three largest correlation coefficients are highlighted for each storm.

A

3 June 2000: Bird City						
Parameter	R_L	Lag	t	90	95	99
VIL	0.78	-1	6.23	1.94	2.45	3.71
30dBZ Height	0.51	-1	2.96	1.90	2.37	3.50
Hail diameter	NA	NA	NA	NA	NA	NA
Hail prob.	0.64	0	4.19	1.90	2.37	3.50
Svr hail prob.	0.72	0	5.16	1.86	2.31	3.36
Rotation	0.44	-1	2.45	1.74	2.11	2.90
cells (45dBZ)	0.64	-2	4.16	1.74	2.11	2.90
45 dBZ Area	0.75	-2	5.67	1.90	2.37	3.50
cells (10 km)	0.47	-2	2.66	1.81	2.23	3.17

B

11 June 2000: Idalia 1						
Parameter	R_L	Lag	t	90	95	99
VIL	0.70	0	4.38	2.35	3.18	5.84
30dBZ Height	0.84	-2	6.92	2.92	4.30	9.93
Hail diameter	0.67	-3	4.04	1.78	2.18	3.05
Hail prob.	0.79	-2	5.76	2.92	4.30	9.93
Svr hail prob.	0.72	0	4.64	1.78	2.18	3.05
Rotation	0.12	1	0.54	2.92	4.30	9.93
cells (45dBZ)	0.76	-3	5.23	2.92	4.30	9.93
45 dBZ Area	0.85	-3	7.22	2.92	4.30	9.93
cells (10 km)	-0.07	3	0.31	1.94	2.45	3.71

C

22 June 2000: Idalia 2						
Parameter	R_L	Lag	t	90	95	99
VIL	0.45	3	3.07	1.90	2.37	3.50
30dBZ Height	0.35	1	2.27	2.02	2.57	4.03
Hail diameter	0.77	1	7.34	2.13	2.78	4.60
Hail prob.	0.62	1	4.81	2.02	2.57	4.03
Svr hail prob.	0.73	1	6.50	2.02	2.57	4.03
Rotation	0.27	-3	1.71	1.86	2.31	3.36
cells (45dBZ)	0.69	2	5.80	2.35	3.18	5.84
45 dBZ Area	0.89	-3	11.9	2.13	2.78	4.60
cells (10 km)	0.70	-1	5.96	2.35	3.18	5.84

D

22 June 2000: Burlington						
Parameter	R_L	Lag	t	90	95	99
VIL	0.84	3	6.38	2.92	4.30	9.93
30dBZ Height	0.93	3	10.4	2.92	4.30	9.93
Hail diameter	0.85	-1	6.65	2.92	4.30	9.93
Hail prob.	0.82	3	5.91	2.35	3.18	5.84
Svr hail prob.	0.85	-1	6.65	2.92	4.30	9.93
Rotation	0.78	0	5.14	2.92	4.30	9.93
cells (45dBZ)	0.76	0	4.82	2.92	4.30	9.93
45 dBZ Area	0.89	1	8.05	2.92	4.30	9.93
cells (10 km)	0.78	0	5.14	2.35	3.18	5.84

E

24 June 2000: Haigler						
Parameter	R_L	Lag	t	90	95	99
VIL	0.41	-3	2.11	1.78	2.18	3.05
30dBZ Height	0.46	-3	2.43	1.73	2.10	2.88
Hail diameter	0.31	-3	1.53	1.83	2.26	3.25
Hail prob.	0.57	-3	3.25	1.73	2.10	2.88
Svr hail prob.	0.29	-3	1.42	1.81	2.23	3.17
Rotation	0.46	1	2.43	1.73	2.10	2.88
cells (45dBZ)	0.41	1	2.11	1.73	2.10	2.88
45 dBZ Area	0.50	-1	2.71	2.02	2.57	4.03
cells (10 km)	0.53	1	2.93	1.78	2.18	3.05

F

29 June 2000: Wheeler						
Parameter	R_L	Lag	t	90	95	99
VIL	0.73	1	5.95	2.35	3.18	5.84
30dBZ Height	0.67	1	5.03	2.92	4.30	9.93
Hail diameter	0.83	0	8.29	6.31	12.7	63.7
Hail prob.	0.58	1	3.96	2.02	2.57	4.03
Svr hail prob.	0.74	-1	6.13	2.35	3.18	5.84
Rotation	0.72	0	5.78	2.92	4.30	9.93
cells (45dBZ)	0.60	-2	4.18	1.90	2.37	3.50
45 dBZ Area	0.86	2	9.38	6.31	12.7	63.7
cells (10 km)	0.43	-2	2.65	1.83	2.26	3.25

ground flashes at the 90% confidence level or better. In the remaining four storms, the three parameters with the highest correlations varied more for ground flashes than for total lightning, but usually included either the maximum estimated hail diameter or hail probability and either the 45 dBZ area or the number of cells within 10 km. Correlations with positive ground flashes typically were better than those with negative ground flashes, typically with correlation coefficients of 0.60–0.75, significant at the 90-95% confidence level. The three best correlation coefficients for negative ground flashes were typically 0.34 – 0.53, significant at no better than the 90% level.

Table 3. Correlations between all cloud-to-ground lightning and radar-inferred storm parameters.

A

3 June 2000: Bird City					
Parameter	**R**	**t**	**90**	**95**	**99**
VIL	NA	NA	NA	NA	NA
30dBZ Height	NA	NA	NA	NA	NA
Hail diameter	NA	NA	NA	NA	NA
Hail prob.	NA	NA	NA	NA	NA
Svr hail prob.	NA	NA	NA	NA	NA
Rotation	NA	NA	NA	NA	NA
cells (45dBZ)	NA	NA	NA	NA	NA
45 dBZ Area	NA	NA	NA	NA	NA
cells (10 km)	NA	NA	NA	NA	NA

B

11 June 2000: Idalia 1					
Parameter	**R**	**t**	**90**	**95**	**99**
VIL	0.29	1.34	2.13	2.78	4.60
30dBZ Height	0.49	2.53	2.35	3.18	5.84
Hail diameter	0.24	1.12	1.77	2.16	3.01
Hail prob.	0.50	2.57	2.35	3.18	5.84
Svr hail prob.	0.38	1.87	1.77	2.16	3.01
Rotation	0.01	0.06	1.77	2.16	3.01
cells (45dBZ)	0.33	1.57	2.35	3.18	5.84
45 dBZ Area	0.45	2.25	1.94	2.45	3.71
cells (10 km)	-0.01	0.03	1.77	2.16	3.01

C

22 June 2000: Idalia 2					
Parameter	**R**	**t**	**90**	**95**	**99**
VIL	-0.02	0.13	2.13	2.78	4.60
30dBZ Height	0.02	0.12	2.02	2.57	4.03
Hail diameter	0.40	2.65	2.13	2.78	4.60
Hail prob.	0.13	0.79	2.13	2.78	4.60
Svr hail prob.	0.29	1.85	2.13	2.78	4.60
Rotation	0.13	0.80	1.86	2.31	3.36
cells (45dBZ)	0.33	2.09	2.35	3.18	5.84
45 dBZ Area	0.76	7.00	2.13	2.78	4.60
cells (10 km)	0.60	4.51	2.92	4.30	9.93

D

22 June 2000: Burlington					
Parameter	**R**	**t**	**90**	**95**	**99**
VIL	0.45	2.06	2.13	2.78	4.60
30dBZ Height	0.49	2.31	2.13	2.78	4.60
Hail diameter	0.50	2.39	2.13	2.78	4.60
Hail prob.	0.46	2.15	1.94	2.45	3.71
Svr hail prob.	0.54	2.62	2.13	2.78	4.60
Rotation	0.48	2.27	2.13	2.78	4.60
cells (45dBZ)	0.26	1.11	2.13	2.78	4.60
45 dBZ Area	0.41	1.88	2.13	2.78	4.60
cells (10 km)	0.27	1.14	1.94	2.45	3.71

E

24 June 2000: Haigler					
Parameter	**R**	**t**	**90**	**95**	**99**
VIL	-0.06	0.27	1.78	2.18	3.05
30dBZ Height	-0.12	0.58	1.73	2.10	2.88
Hail diameter	-0.14	0.64	1.78	2.18	3.05
Hail prob.	-0.22	1.05	1.73	2.10	2.88
Svr hail prob.	-0.03	0.15	1.78	2.18	3.05
Rotation	-0.17	0.81	1.73	2.10	2.88
cells (45dBZ)	-0.13	0.63	1.73	2.10	2.88
45 dBZ Area	-0.58	3.36	1.83	2.26	3.25
cells (10 km)	-0.29	1.39	1.73	2.10	2.88

F

29 June 2000: Wheeler					
Parameter	**R**	**t**	**90**	**95**	**99**
VIL	0.50	3.21	2.13	2.78	4.60
30dBZ Height	0.57	3.84	2.92	4.30	9.93
Hail diameter	0.64	4.61	2.92	4.30	9.93
Hail prob.	0.36	2.12	1.83	2.26	3.25
Svr hail prob.	0.61	4.24	2.35	3.18	5.84
Rotation	0.62	4.46	2.92	4.30	9.93
cells (45dBZ)	-0.25	1.46	1.90	2.37	3.50
45 dBZ Area	0.82	8.04	2.92	4.30	9.93
cells (10 km)	0.04	0.22	1.90	2.37	3.50

2.3. Storm Simulation Study

The University of Oklahoma and National Severe Storms Laboratory jointly developed a numerical cloud model that includes electrification processes and lightning, to study electrification and lightning in several storms (e.g., Mansell 2000, MacGorman et al. 2001, Mansell et al. 2002, Mansell et al. 2005). One emphasis of these and other simulation studies has been to evaluate relationships of lightning with various storm properties, such as graupel mass and volume, cloud ice mass and volume, maximum updraft, and updraft mass flux through a particular level in the mixed phase region. Our most recent study is presented here. The relationships found in this study corroborate and extend relationships that were found in previous studies

The present study focuses on numerical simulations of the 29 June 2000 supercell storm that occurred during the field project of STEPS and is one of the storm also discussed in the previous section.. The 29 June supercell storm produced an F1 tornado, large cloud flash rates, and predominately positive ground flashes.

An in-depth study of storm processes proceeds from a combination of observations and numerical simulations. STEPS provided a comprehensive observational data set for detailed comparison with numerical simulations of storm evolution. The objective is to evaluate how well the simulated charge structure, lightning flashes, updrafts, and precipitation structure reproduce key observed features of the actual storm. The relationships between the modeled total flash rate and other storm characteristics are of particular interest.

Laboratory experiments have attempted to duplicate the process of charge transfer in storms. The laboratory studies have shown that temperature, liquid water content, the sizes of the particles and the riming rate all exert important influences on charging. Reynolds et al. (1957) and Takahashi (1978) were among the first to examine the charge separated per rebounding collision of graupel and liquid water and graupel and ice to determine how hydrometeors obtained charge. Jayaratne et al. (1983) and Keith and Saunders (1990) also investigated charge separation, including dependency on crystal size, impact velocity, and contaminants in water particles. A broad agreement is noticed between the laboratory results, with differences depending on the laboratory apparatus used (Jayaratne 1993; Pereyra et al. 2000), the growth mode of the ice crystals, and the liquid water content (MacGorman and Rust 1998, pgs. 67-9).

Several studies have used numerical cloud models to further test the implications and accuracy of laboratory measurements. Takahashi (1983, 1984) parameterized his laboratory noninductive charging data in a two-dimensional, time dependent axisymmetric model study of small thunderstorms. Mitzeva and Saunders (1990) added a parameterization of the laboratory results of Jayaratne et al. (1983) and Keith and Saunders (1990) to a one-dimensional model to examine the evolution of charging rates in three different simulations. Ziegler et al. (1986) used a one-dimensional kinematic model with an electrification mechanism suggested by Gardiner et al. (1985). The study was expanded to three-dimensions with time dependence and a parameterization of the screening layer (Ziegler et al. 1991), which was later applied by Ziegler and MacGorman (1994) to study a supercell storm. Mansell (2000) and Mansell et al. (2002) developed a lightning parameterization using a stochastic dielectric breakdown model that simulates the stepwise propagation of individual flashes and reduces the electric field by realistically redistributing charge in the model domain.

Correlations of flash rate with updraft dynamics and various microphysical properties have been the focus of many studies as flash rate is often considered an indication of storm severity. High reflectivity (Lhermitte and Krehbiel 1979, MacGorman et al. 1989), increasing graupel volume (Carey and Rutledge 1996) and production of large hail (Carey and Rutledge 1998) have all been related to larger flash rates in observational studies. One of the most obvious and perhaps important parameters

controlling flash rate is the storm size (Williams 2001). Large storms tend to have a higher sustained flash rate due to a stronger updraft (MacGorman et al. 1989), though smaller storms with strong updrafts have also been observed to have relatively high flash rates. In a simulation study with a one-dimensional model, Baker et al. (1995) and Solomon and Baker (1998) examined the total flash rate in conjunction with updraft speed, reflectivity, precipitation rate, ice concentration, and cloud radius.

There has been considerable discussion concerning cloud-to-ground flashes and their relationship to the charge distribution and severity of storms. Several observational studies have found that the first cloud-to-ground lightning flash tends to lag cloud flashes in storms and tend to begin as the strong reflectivity core descends (e.g., Larson and Stansbury 1974 and MacGorman et al. 1989) or as strong downdrafts approach the ground (Goodman et al. 1988, Williams et al. 1989, Watson et al. 1991). Simulations have demonstrated similar trends, due to these properties' influence on the formation of the lower charge region thought necessary to initiate cloud-to-ground flashes (MacGorman et al. 2001 and Mansell et al. 2002).

This study examines the consequences of different charge separation mechanisms on simulated electrification and compares the simulated charge structures to the observed charge structure of the well-documented 29 June 2000 STEPS storm. An analogous study has been performed using a two-dimensional model of a mountain storm (Helsdon et al. 2001), in which three different noninductive charging schemes were examined. However, the storm simulated by Helsdon et al. (2001) was not compared in detail with observed storm characteristics. Mansell et al. (2005) and Mansell et al. (2002) also tested different numerical parameterizations of noninductive and inductive charging in relation to smaller, multicellular storms.

The present study employs a three-dimensional model to determine which charging scheme(s) provide results similar to the observed morphology of 29 June and to further examine the relationships between flash rate and other storm properties such as updraft speed and mass flux, precipitation rate, graupel volume, and rain mass. This study also examines multiple positive CG flashes that occurred at various times during both the simulations and the observed storm and relates these positive CG flashes to the evolving kinematic, microphysical and electrical structure of the storm.

2.3.1 Model Description

2.3.1.1. Dynamics and microphysics

The dynamic cloud model is described in detail by Straka (1989) and Carpenter et al. (1998). The model is three dimensional, non-hydrostatic and fully compressible, and is based on the set of equations from Klemp and Wilhelmson (1978). The model includes prognostic equations for velocity components (momentum), perturbation pressure, potential temperature, turbulent kinetic energy, water vapor and hydrometeor mixing ratios, rime history, and charge variables.

The model's microphysics package includes two liquid hydrometeor categories and ten ice categories distinguished by particle density, habit, and size (Straka and Mansell 2005). Fractions of mass may move from one category to another. The fraction moved depends on droplet collection, riming rate, and melting. Source and sink terms for form and phase changes are included in the microphysics scheme for condensation and evaporation, deposition and sublimation, freezing and melting, aggregation and nucleation, and riming of ice particles, graupel and hail.

2.3.1.2. Charging and electrification

The electric potential is determined from the net charge (i.e., the sum of all charge at a grid point, taking into account charge polarity) at every point in the domain by Poisson's equation, and

the electric field is determined as the negative gradient of the potential: $\mathbf{E} = -\nabla\varphi$. Charge sources include fair-weather ion production, hydrometeor charging, corona current from the ground, diverging electric currents produced by storms, and lightning. The model includes a choice of parameterizations for charging hydrometeors (Mansell et al. 2005), including parameterizations for both inductive and noninductive charging. Each simulation typically includes one noninductive parameterization and one choice of inductive charging parameters, as well as charging from other sources. The results of laboratory and modeling studies strongly suggest that noninductive charging plays the primary role in producing electrification levels close to the levels observed in storms (MacGorman and Rust 1998). However, it has been suggested that inductive charging can also play a role (e.g., Brooks and Saunders 1994).

1) Inductive charging parameterization

Inductive charging occurs in the presence of an electric field, during a rebounding collision occurs between two polarized particles. In the model, inductive charging occurs only for collisions involving graupel and droplets, and then only when graupel is in "dry-growth" mode. Noninductive charging (independent of the electric field) occurs during rebounding collisions between riming graupel and ice particles in the presence of liquid water. In a given region, the charge gained by graupel is equal and opposite to the charge gained by cloud particles, so microphysical charging does not by itself produce regions of net thunderstorm charge. Graupel and cloud particles have different fall speeds, and this differential sedimentation separates the charge on macroscopic scales to create regions of net charge, eventually resulting in large electric fields and lightning.

Inductive charging in the model is calculated based on a formula from Ziegler et al. (1991). The inductive charging used in the present 29 June supercell simulations approaches values described as "strong" by Mansell et al. (2005).

2) Noninductive charging parameterizations

As discussed above, noninductive charging involving riming graupel and ice crystals has been the focus of several laboratory experiments. The charge gained by the graupel is dependent on the ambient temperature and the liquid water content as well as the size and growth state of the hydrometeors. Many studies have focused on determining a reversal temperature for the transition in the sign of charge gained by graupel. Most studies agree that the reversal temperature is dependent on the liquid water content or riming rate, though differences arise in determining the conditions for charge sign reversal.

For this study, the model includes four different parameterizations of the noninductive charging process. Each varies at least a bit in how it determines the sign and magnitude of graupel charging. For all parameterizations in our model, the magnitude of charge exchanged by individual graupel and cloud particle collisions $|\delta q|$ is limited to a maximum of 50 fC for graupel-snow collisions and 20 fC for graupel-cloud ice collisions, to prevent unrealistic charging and lightning flash rates.

One parameterization of the noninductive charging rate is based on the laboratory results of Saunders and Peck (1998). As shown in Fig. 6a, the magnitude and sign of charging in this scheme (SP98) depends on a graupel particle's rime accretion rate (RAR). The reversal temperature also varies with RAR. Equivalently, one can consider that the reversal in the polarity of graupel charging at a particular temperature occurs at a critical RAR value (RAR_{crit}), and RAR_{crit} varies with temperature. The sign of the charge transferred to the graupel during a rebounding collision in the SP98 scheme is strongly influenced by the amount of water accreted on the graupel (i.e. on the rimer).

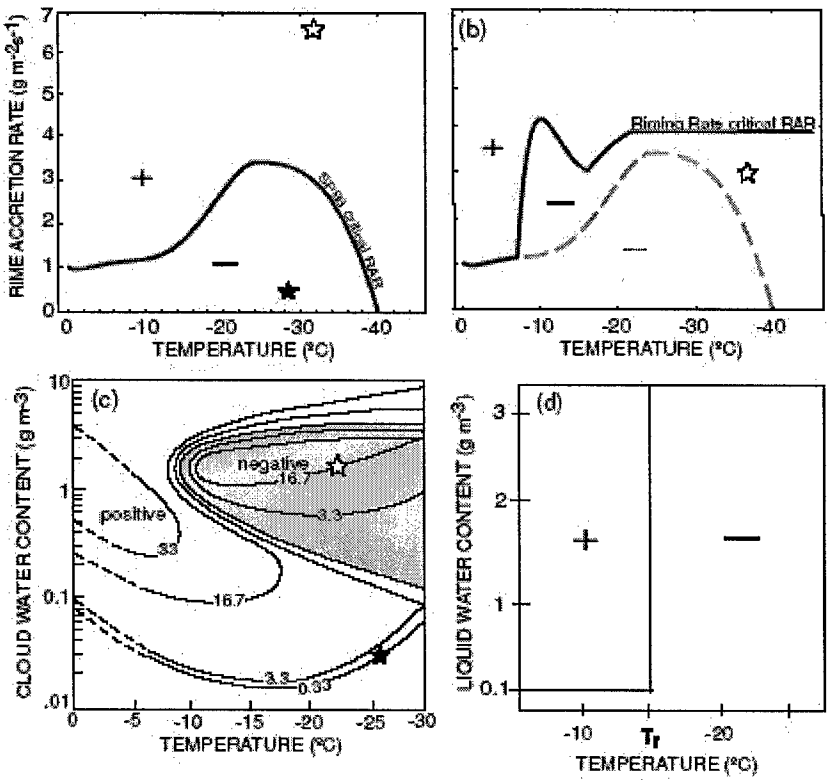

Figure 6: (a) The polarity of charge gained by graupel as a function of temperature and RAR according to the laboratory experiments of Saunders and Peck (1978). Graupel gains positive charge above the curve at higher rime accretion rates and negative charge below the curve. (b) The polarity of charge gained by the graupel as a function of temperature and RAR according to the RR scheme. (The SP98 scheme is shown again for comparison.) (c) The polarity of charge gained by graupel as a function of temperature and cloud water content, adapted from Takahashi (1978). (d) Polarity of the charge gained by graupel during GZ simulation as a function of the reversal temperature and liquid water content.

The second parameterization is the Riming Rate (RR) scheme, as described by Mansell et al. (2005). This parameterization is similar to SP98 and is also based on a critical rime accretion rate. However, its dependence on temperature and RAR, shown in Fig. 6b, is somewhat different from that of SP98.

The third is the Takahashi (TAKA) charging scheme, based on the laboratory work of Takahashi (1978). The magnitude and polarity of charge gained by graupel is determined by the temperature and liquid cloud water content, as shown in Fig. 6c. In our parameterization, the charge per collision is taken from a lookup table developed by Wojcik (1994), with additions from Takahashi (1984) to account for the dependence on impact velocity and ice crystal size. The charge separated per collision at temperatures between 0°C and -30°C and at liquid water contents from 0.01 to 30 gm^{-1} are included in the table. At temperatures below -30°C the charge separated per collision is the value at -30°C.

The final noninductive parameterization used by this study is the Gardiner/Ziegler (GZ) scheme. This scheme is based on the laboratory results of Jayaratne et al. (1983), as adapted from Gardiner et al. (1985) by Ziegler et al. (1986, 1991). The magnitude and sign of charge which graupel gains is governed by an adjustable reversal temperature and by the cloud water mixing ratio. The reversal temperature remains fixed for a given simulation, and for this study, it was set to -15°C, as shown in Fig. 6d.

3) Charge conservation, advection, and ions

Once electrification begins, a charge density is connected with every hydrometeor type. As mass shifts between categories in the microphysics, the associated charge also is transferred from one category to another (e.g., mass from ice to rain). Although charge is conserved in the model domain, charge is not absolutely conserved due to ion currents entering or exiting the domain, charge advection through a lateral boundary, or charge removal by cloud-to-ground lightning. The charge continuity equation from Mansell et al. (2005) resembles a typical conservation equation with treatment of advection, diffusion, and falling particle motion. The model neglects the accelerations of charged particles in an electric field.

Explicit treatment of ions has recently been added to the OU-NSSL model by Mansell et al. (2005). Conservation equations are defined for both positive and negative ion concentrations. The equations take into account advection and mixing, drift motion (ion motion induced by the electric field), cosmic ray generation, ion recombination, ion attachment to hydrometeors, corona discharge from the surface, and release of ions from evaporating hydrometeors. Mansell et al. (2005) use a fair-weather state for background ion generation and destruction from Gish (1944), as expressed by Helsdon and Farley (1987), in addition to thunderstorm sources and sinks.

4) Lightning parameterization

Lightning flashes are parameterized by a stochastic dielectric breakdown model as described in Mansell et al. (2002). The lightning develops bidirectionally across a uniform grid with each step chosen randomly from among the surrounding points at which the electric field meets or exceeds a threshold value for propagation. After each step, the electric field is calculated to determine the contribution by the lightning channel. The end result is a branched or fractal-like leader structure of each flash in three dimensions.

Flash initiation occurs if the electric field exceeds a macroscopic threshold of E_{be}. A particular initiation point is chosen randomly from all the points that exceed $0.9E_{be}$ and each channel maintains an overall charge neutrality as long as neither end goes to ground. Positive leaders carry positive charge and travel preferentially through negative charge regions, while negative leaders carry negative charge and tend to travel through regions of net positive charge (Mansell et al. 2002). Therefore, the simulated flashes tend to reflect the simulated charge structure.

2.3.2. Observations of the 29 June 2000 Supercell Storm

The 29 June 2000 supercell storm formed just ahead of a dryline, with an approaching mesoscale cold front to the north. The environment was unstable, with 1319 J kg^{-1} of convective available potential energy (CAPE), but was also strongly capped, with convective inhibition (CIN) of about 100 J kg^{-1}. Strong 0 to 3 km storm relative helicity (SRH) indicated the support for the development of rotating updrafts during the supercell phase of the storm.

The storm formed near the border intersection of Colorado, Nebraska and Kansas. It propagated southeastward through northwest Kansas for approximately 4 h before being overtaken by part of a mesoscale convective system (MCS) in central Kansas later that evening. During the first three hours, the storm produced large hail, an F1 tornado, and a profuse amount of lightning. As it

propagated through the STEPS domain, observations were taken from a network of Doppler radars, a T-28 armored research airplane traversing through the storm, balloon soundings of the electric field, and the Lightning Mapping Array (LMA).

On radar, the storm first appeared as a small echo at approximately 2130 UTC. By 2305 UTC, the storm contained a strong updraft and high reflectivities, though it was still multicellular in nature, with various dominant updrafts. At approximately 2330 UTC, the storm made a right turn toward the south-southeast and slowed (Fig. 7). It rapidly intensified and grew in area at all levels, as the updraft volume increased from 70 km^3 to 110 km^3 in about 0.5 hour. During this period, the Doppler-derived maximum updraft speed was near 50 m s^{-1} (Tessendorf and Rutledge 2002), and the storm assumed a supercell structure, sometimes including a bounded weak echo region (BWER) on the western or southwestern flank, as shown in Fig. 8.

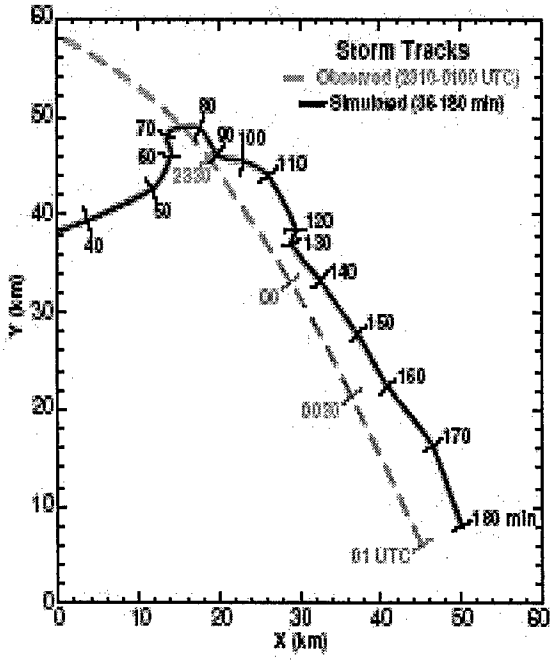

Figure 7. Observed (dashed gray line) and simulated (solid black line) storm track for the 29 June 2000 supercell storm.

Figure 9 shows the observed lightning flash rates. The first lightning detected by the LMA in the storm was at 2150 UTC. The first cloud-to-ground flash (CG) was detected by the NLDN almost 50 minutes later, at 2239 UTC, and only two more CG flashes occurred over the next 40 minutes. Prior to the storm turning rightward, the lightning flash rate was 20 per minute. Both in-cloud (IC) and CG flash rates increased rapidly, as the storm turned to the right. By approximately 0015 UTC, the storm reached a maximum of 300 flashes per minute. During the first three hours, the storm produced a total of roughly 10,000 flashes, 159 of which were CG flashes. The first ground flash and approximately 90% of the CG flashes observed during this period were positive.

2.3.3. Model Simulation of the 29 June 2000 Supercell Storm

2.3.3.1. Storm initiation

The supercell storm was initiated on an 80 by 80 by 20 km domain. Horizontal grid spacing was 1 km grid, and vertical grid spacing stretched from 200 m near the surface to 500 m aloft. The model environment was determined by using a modified version of the NCAR mobile GLASS sounding from Goodland, KS. The sounding was modified in the convective boundary layer (CBL) by increasing the temperature and moisture to better depict the environment where the storm initiated as indicated by surface observations. This modification was consistent with mobile mesonet observations in the vicinity of the storm, which recorded higher temperatures and dewpoints than the mobile sounding earlier that day (E. Rasmussen, personal communication, 2004). The base of the elevated residual layer capping the moist CBL was warmed adiabatically to maintain a minimum concentrated cap strength, thus controlling the spurious convection and preserving the mixed layer.

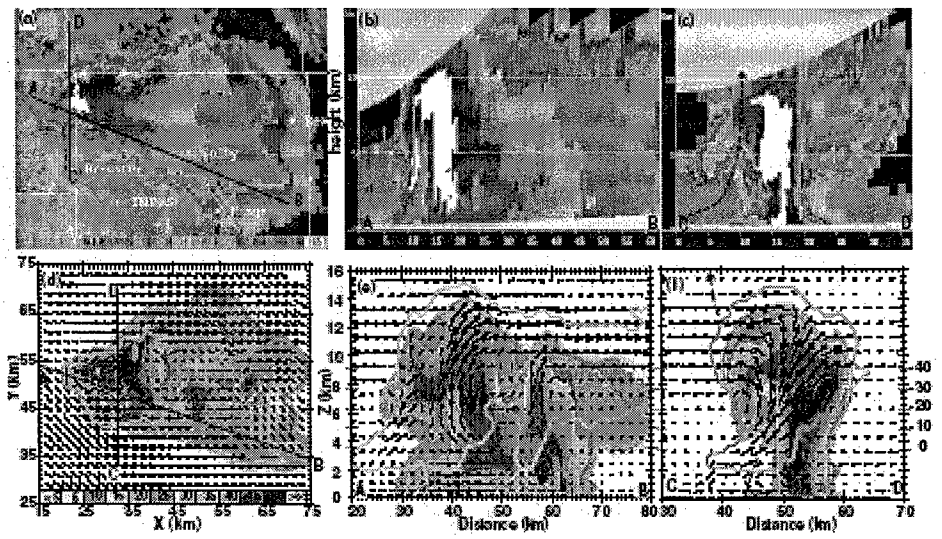

Figure 8. Top row: Radar reflectivity from the Goodland, KS, WSR 88D radar at 0004 UTC. The path of the balloon launched at 0004 UTC is depicted by a dashed black line. (a) 0.5-deg elevation scan. Cross-sections for (b) and (c) are denoted by solid black lines. (b) Vertical cross-section along line AB. (c) Vertical cross-section along line CD. Bottom row: Reflectivity, ground relative wind vectors, and cloud outline (grey) from the simulation at 116 min. The path of the simulated balloon is depicted by a dashed red line that began at 113 minutes. At 116 minutes, the balloon was just below 2 km. (d) X-Y planar view at an altitude of 6.8 km. (e) Vertical cross-section along line AB. (f) Vertical cross-section along line CD. Maximum updraft speed is 54.5 m s^{-1}.

The instability of the environment in the modified sounding was thus greatly increased, the CAPE rising from 1370 J kg^{-1} to 2875 J kg^{-1} and the CIN lowering from 100.3 J kg^{-1} to 22.1 J kg^{-1}. The Bulk Richardson Number (BRN), defined as the ratio of the CAPE to the lower tropospheric vertical wind shear, increased from 10.3 to 23.1. The CAPE and BRN of the modified sounding were supportive of possible supercell development (Weisman and Klemp 1982). The model environment was assumed to be horizontally homogeneous. A warm bubble ($\delta T = 3$ K) with randomized thermal perturbations and a radius of 9–11 km was used to initiate the storm simulation.

2.3.3.2. Dynamical and microphysical evolution

The model allows no feedback from the electrification to the microphysics or dynamics; therefore, each of the four simulations had exactly the same dynamical and microphysical evolution. The simulated storm initially developed an elongated multicell structure, with successive main updraft cores along the edge of the outflow on the upshear side. By 76 min, the storm developed a solid core of reflectivity extending to ground, with a deep updraft and forward anvil region. During the first 90 minutes, the storm moved towards the east-northeast (Fig. 7). By 90 minutes, it appears that storm rotation and the cold pool had intensified sufficiently to force the storm to turn right towards the south and decelerate. The storm continued along a south-southeasterly track for the remainder of the simulation.

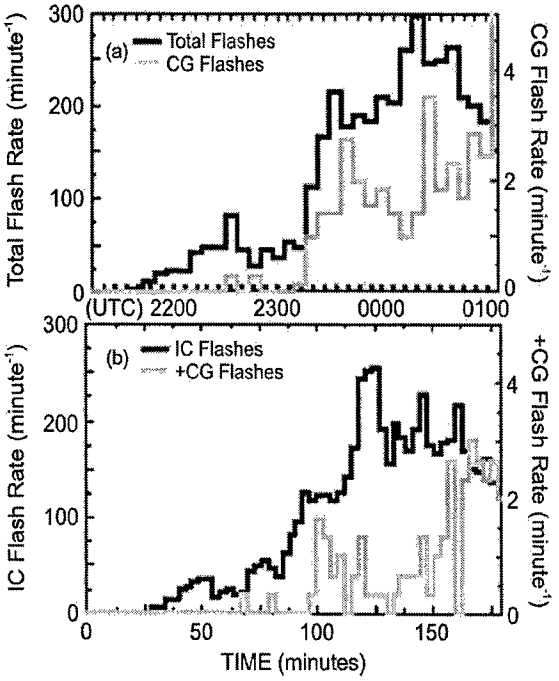

Figure 9. Observed and simulated lightning flash rates (minute^{-1}) for the 29 June 2000 STEPS storm. (a) Total flashes detected by the LMA (black line) and total cloud-to-ground (CG) detected by the NLDN (gray line). (Adapted from Wiens et al. 2003). (b) In-cloud (IC) flashes (black) and CG flashes (grey) from SP98 noninductive charging.

The timing of the right turn is the point from which we compared the simulated and observed storms. The initial development of the observed storm was much slower than that of the simulation, but from the time of the right turn onward, the development of the simulated storm agrees reasonably well with that of the observed storm. This agreement is significant in that most of the total lightning and virtually all the CG flashes occurred after the right turn in both the simulations and the observed storm.

The maximum updraft speed of the simulated storm reached 30 m s^{-1} at 16 min and remained stronger throughout the rest of the simulation, with a peak of 61 m s^{-1} at 147 min. The simulated supercell exhibited evidence of convective surges during its life cycle. The first growth phase occurred at approximately 20 minutes with increases in updraft mass flux, updraft volume, and graupel volume. (Updraft volume and graupel volume are shown in Figs. 10 and 11.) Another convective surge occurred as the storm track turned more southerly. This surge resulted in the simulated storm becoming a supercell similar to the observed storm, as shown in Fig. 8. The maximum strength of the storm occurred between 140 and 160 min, when a simulated reflectivity maximum of 69 dBZ was attained. Updraft mass flux and graupel volume also reached a peak during this time.

2.3.3.3. Evolution of electrical properties (Saunders and Peck noninductive charging)

The results from Saunders and Peck (SP98) and the Rime Accretion Rate (RAR) parameterizations agreed best with observations of lightning activity. Because results from SP98 and RAR were similar, we will focus on only one, SP98, in the remainder of this treatment. As described previously, the sign of the Saunders and Peck (SP98) noninductive charging is dependent on the rime accretion rate (the amount of liquid accreted on the rimer) and the temperature of the air. The magnitude of the charge separated also depends on crystal size and impact speed.

The large liquid water content in the initial updraft caused transfer of positive charge to graupel to dominate the charge produced by the SP98 scheme in the simulation. This produced a mid-level positive charge with an upper negative charge (an inverted dipolar structure) at 28 min. The inverted dipole was replaced by an inverted tripolar structure at about 35 min, as inductive charging and precipitation recycling and fallout quickly developed a lower negative charge region for the third layer. The inverted tripolar structure persisted for much of the initial stages of the storm, with all three charges eventually extending horizontally through much of the storm. Corona from the round produced a positive charge layer below 0.5 km AGL by 76 minutes.

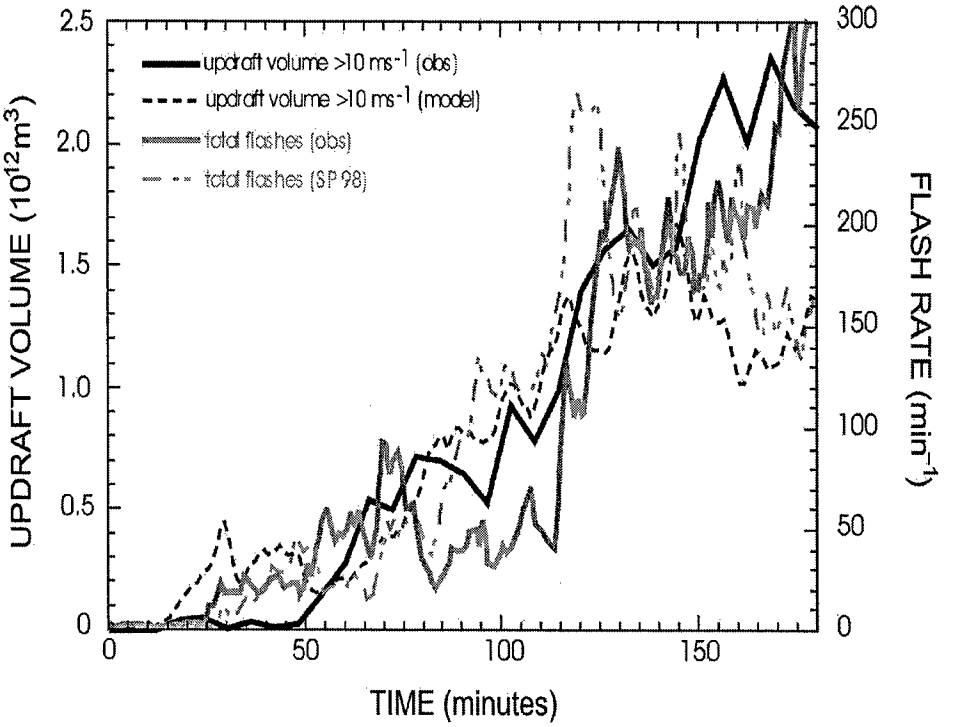

Figure 10. Total flash rates and updraft volume observed (Tessendorf and Rutledge 2002) and simulated for the 29 June 2000 supercell storm.

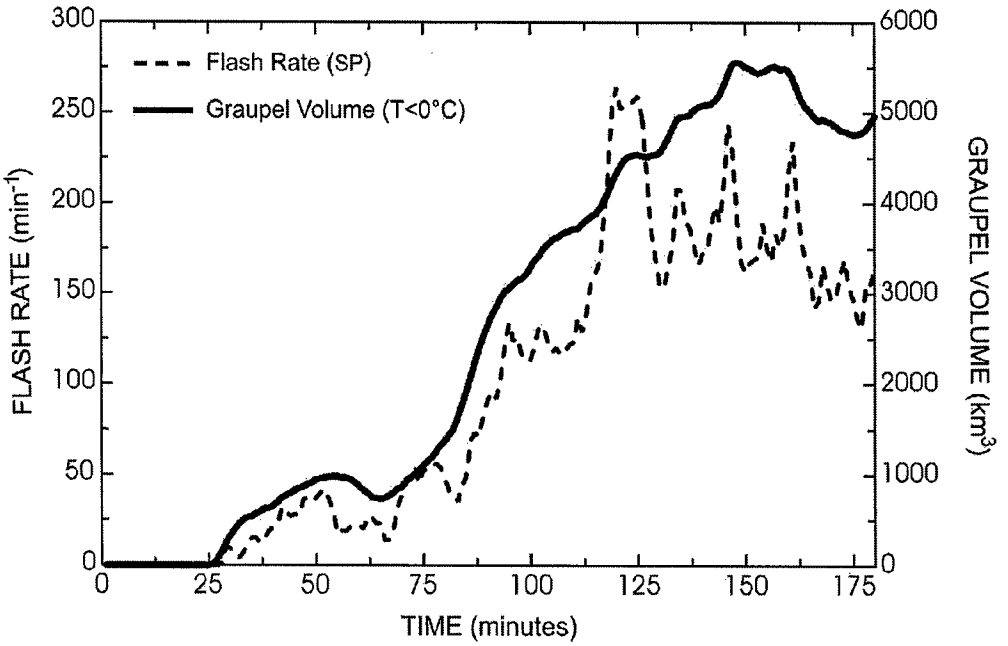

Figure 11. Graupel volume and total flash rate (SP98) from the 29 June supercell simulation.

By 116 minutes, the mature stage of the storm had a very complex charge distribution, with opposite charges occurring at the same altitude. The updraft and reflectivity core regions continued to maintain a tripolar structure, but outside this region there were five or more vertically stacked regions. The overall charge structure was similar to that of an inverted-polarity storm, as observed by Marshall et al (1995), Rust and MacGorman (2002), and Rust et al. (2005).

As shown in Figs. 9–10, simulated intracloud (IC) flashes in the SP98 simulation began at 28 minutes, with a flash rate of approximately 30 minute^{-1} throughout the rest of the first hour. Shortly before the storm turned to the right, flash rates increased rapidly to over 100 minute^{-1}. The IC flash rate reached a maximum of 264 minute^{-1} at 120 minutes and maintained a flash rate greater than 150 minute^{-1} during the remainder of the simulation. Lightning leaders traveled preferentially through layers of opposite charge, with positive leaders concentrated in negative charge near 5 km and 13 km. Middle levels of the storm were dominated by negative leaders traveling through positive charge.

The SP98 scheme produced a total of 98 positive ground flashes, the first occurring at 67 minutes (Fig. 8). No negative ground flashes were produced. The CG flashes typically initiated between 5 and 7 km AGL, between the main positive charge region and a lower negative charge region. In the simulation, positive CG flashes were produced by a negative leader traveling upward through positive charge and a positive leader traveling downward past negative charge to ground. Most simulated lightning flashes exhibited considerable branching by lightning leaders from the point of initiation. On occasion, a leader went directly to ground beneath the point of initiation, but often a flash went to ground more than 1 km horizontally from its initiation point. The direction of the path of leaders to ground depends on the distribution of charge surrounding the leader as it develops. The majority of the CG strikes were located just downshear of the main convective core, though some occurred directly under the main updraft.

To evaluate the electrical structure of the storm, we compared the vector electric field measured by a balloon that ascended through the storm (MacGorman et al. 2005) with the electric field measured by a simulated balloon released into the main storm updraft at 113 minutes. The simulated EFM was released at approximately the same time during the storm's life cycle as the actual EFM sounding and followed roughly the same track up to an altitude of 12 km AGL. Above that altitude, the simulated balloon continued to ascend through the cloud top, but the observed balloon was punctured and began to descend. The observed and simulated profiles of temperature and relative humidity (with respect to liquid water) were remarkably similar below 12 km. Both soundings were contained within updraft regions and found little charge below 8 km. An inverted tripole charge structure was observed in the simulated balloon sounding during the SP98 and RR simulations, and the height and magnitude of the upper negative and main positive charge regions were similar to those of the corresponding regions from the observed storm. The lower charge in the tripole, a small lower negative charge region near 8 km, was not revealed in the observed updraft sounding, though observed during the descent. The simulated sounding may have been closer than the observed sounding to precipitation, which contained the lower negative charge region in the observed sounding.

The simulated soundings from the TAKA and GZ simulations depicted a normal tripolar charge structure. This was opposite to the inverted tripole of the SP98 and RR simulations and opposite to the observed sounding. Thus, in this case, the SP98 and RR simulations were more realistic, though they may not be for other storms.

The observed descending electric-field profile from 29 June was much more complex than found in the updraft region. Based on the electric field profile, it was estimated that four or five levels of charge were present in the rainy downdraft, instead of the two or three charge layers observed in

the updraft core. A similar profile was also noted in the model outside the updraft regions, where pockets of charge added complexity to the profile.

2.3.3.4. CG production relative to storm microphysics and kinematics

As discussed above, updraft properties and precipitation growth in the mixed phase region govern the overall electrification and lightning activity of storms. This explains the strong relationship between total lightning activity and the intensity and size of storms in both observations and simulations. However, producing cloud-to-ground lightning requires something besides strong electrification. All of our storm simulations and several observational storm studies suggest that producing cloud-to-ground lightning usually requires the formation and descent of substantial precipitation to lower levels of the storm (at least warmer than -10 °C). The lowering of precipitation permits the formation of a lower charge opposite in polarity to the main charge region just above it. This lower charge increases the electric field in the lower part of the storm enough to initiate lightning, but is not large enough to cause lightning to stop within the charge region. Instead, the lightning continues past the charge to ground.

The general degree of electrification will modulate ground flash activity, but the additional requirement to produce ground flash activity means that ground flash rates may not be commensurate with the overall degree of electrification. In fact, ground flash rates have been found to have little relationship with storm severity or updraft strength (e.g., Reap and MacGorman 1989). One must rely on cloud flash rates or total flash rates to provide such a relationship.

2.3.3.5. Total flash rate relative to storm microphysics and kinematics

The total flash rate appears to be the best electrical representation of the intensity and microphysical activity of the storm. Of the various microphysical parameters we examined, graupel volume had the best correlation with lightning flash rates in both the observed storm and the simulations (e..g, Figs. 11 and 12). Suggestions of pulses in the total flash rate occur at different periods of the storm. As the graupel volume or mass flux through the updraft increases, the collisions occurring between graupel and ice particles also increase. Consequently, noninductive charging and electrification increase, forcing the flash rate to increase to keep the larger electric field magnitudes in the storm under control. Evolution of the updraft volume through the mixed phase layer also shows similarities between the flash rate in both the model and observations (Fig. 10).

The relationship between total lightning activity and other indicators of storm intensity is valid on two time scales, both over the whole storm life cycle and over the shorter cycles within it. The strong appearance of a relationship in Figs. 10 and 11 is dominated by the continuous growth of the storm during the three hours of the simulation. All parameters increased fairly steadily throughout most of the period.

To show the relationships over smaller convective cycles, it is necessary to remove the linear trend from each storm parameter. Following the statistical methods of MacGorman et al. (1989), an unbiased cross-correlation estimate still reveals a strong relationship between the variables after the linear trend is removed (Fig. 12 and Table 4). Graupel volume and total lightning show a strong correlation at approximately zero time lag. Updraft mass flux and updraft volume suggest a maximum correlation with total lightning lagging by about 10 min. It is apparent in both the model simulations and the observed storm that the total flash rate closely models storm intensity. Thus, total flash rate is perhaps the best electrical representation of the evolving size and severity of the 29 June STEPS supercell storm and simulations.

Table 4. Correlations of lightning flash rates with various storm parameters after linear trends were removed. Correlation coefficients are given for each of the four noninductive parameterizations that were used in a simulation.

Storm Parameters	Correlation Coefficient with Total Flash Rate			
	SP98	RR	TAKA	GZ
Graupel Volume (T < 0°C)	0.770	0.706	0.721	0.808
Updraft Mass Flux (T = -20°C)	0.533	0.482	0.513	0.561
Updraft Volume (w > 10 m s^{-1})	0.650	0.595	0.626	0.686
Maximum Updraft Speed	0.091	0.090	0.098	0.075

2.3.4 Summary of Simulation Results

The simulated storm charge structure is dependent on which noninductive charging parameterization is used. The two schemes based on rime accretion rate (SP98 and RR) both produced inverted polarity thunderstorm charge structure, which appears to provide the best overall agreement with electrical observations from 29 June. However, these parameterizations also develop inverted polarity charge distributions in a wide range of other environments, many of which actually produce normal polarity charge distributions. The liquid water content scheme (TAKA) and the

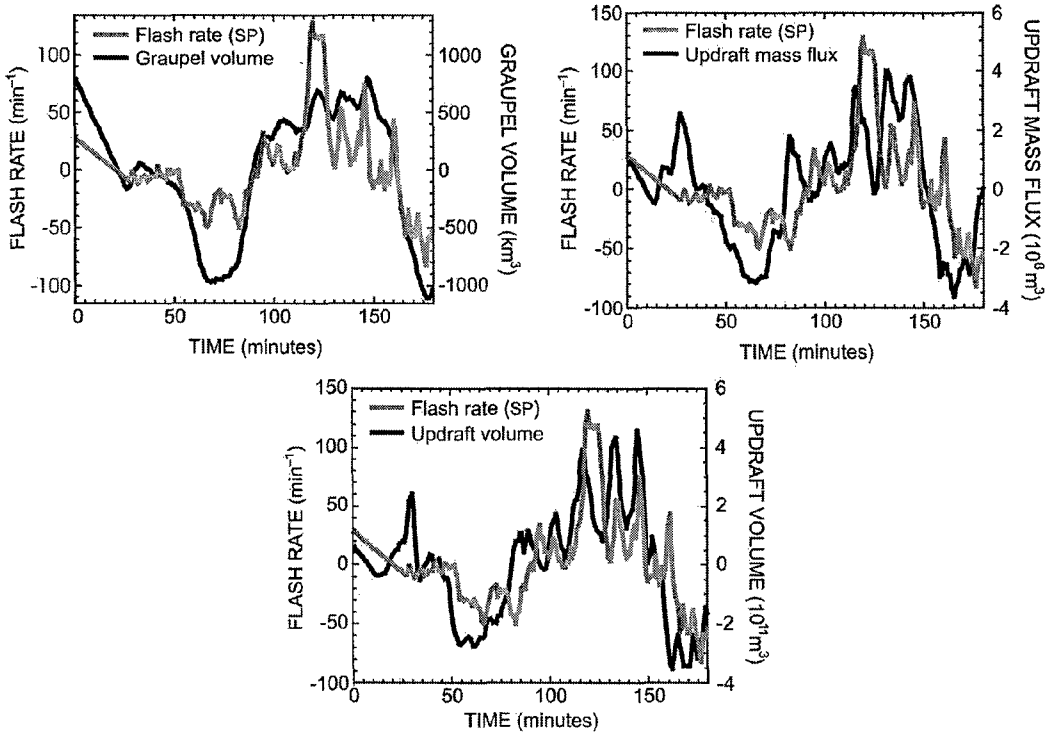

Figure 12. Time-series plots of the total flash rate and various other storm parameters after linear trends were removed.

simpler temperature reversal scheme (GZ) developed normal polarity charge distributions and tend to do so in most environments. Thus, it appears likely that the magnitude and polarity of charge produced by the noninductive mechanism probably is affected by some parameter not yet included in the laboratory experiments used as the basis for our parameterizations. Though this uncertainty affects conclusions that can be drawn from our simulations, the broad trends in the relationship of the simulated lightning rates to other storm parameters such as graupel volume and updraft volume are affected relatively little.

Simulated lightning flashes had morphological characteristics and statistical variability similar to those of observed flashes. In both LMA observations and in model simulations, normal-polarity cloud flashes initiated below positive charge and above negative charge and inverted-polarity flashes initiate below negative charge and above positive charge. In all cases in which positive ground flash initiation could be observed in sufficient detail in the LMA data, it appeared that initiation occurred in the convective core only when the lowest charge was negative, as was the case in the simulations. The occurrence of ground flashes in the simulations appeared to be associated with charge descending into very low regions of the storm, possibly corresponding to descending precipitation cores, as has been reported by MacGorman et al. (1989) and Carey and Rutledge (1996). However, accurately diagnosing the location and timing of ground flash activity is problematic, because the stochastic nature of lightning initiation and propagation prevents knowledge of where a particular flash will propagate or even whether a flash that initiates in a favorable region will reach ground.

As suggested by several observational studies (e.g., Lhermitte and Krehbiel 1979, Williams et al. 1989), the total flash rate of the storm simulations was positively correlated with fluctuations in the intensity of convection and precipitation. These correlations were forced by the noninductive charging and the subsequent three-dimensional motions of the charged hydrometeors. Observational studies and the simulations both show that the total flash rate, instead of ground flash rate or storm polarity, provides the best electrical diagnostic of the microphysical and kinematic intensity of a storm.

Task 3. Develop techniques for assimilating data from all types of lightning into numerical mesoscale forecast models.

3.1. Background

Recent studies have shown that forecasts can be improved by using a more accurate specification of deep convection during the initialization period of mesoscale forecast models. For example, from model experiments that used subjective analyses to improve initial conditions, Stensrud and Fritsch (1994a) suggested that forecasts could be improved by a data assimilation procedure that includes "the effects of parameterized convection, as indicated by radar or satellite during the assimilation period..." as well as explicit representation of boundary layer (BL) cold pools from ongoing storms as diagnosed from surface observations. Stensrud and Fritsch (1994b) demonstrated that explicitly introducing storm-induced cold pools into the mesoscale initial condition improved the mesoscale quantitative precipitation forecast (QPF) by improving the triggering of ongoing convection forced by those cold pools. However, it is recognized that data assimilation is not a panacea for all problems of forecast models. The greatest improvements in forecasts from assimilating data that depict convection should occur in environments where storms have a significant impact on near-future convection and the mesoscale environment of the convection, such as by generation of outflow boundaries and mesoscale upper tropospheric outflow (anvil) plumes (as in the

case studied by Stensrud and Fritsch 1994b).

Though Stensrud and Fritsch (1994a) suggested assimilating radar or satellite data, it would be possible to use any type of data that provides the location of convection and also, preferably, a measure of its intensity. Lightning data satisfy these criteria and have the following additional advantages: compactness (i.e., low bandwidth); ability to unambiguously locate deep convection; detection in mountainous areas and beneath high cloud; and long-range detection of storms over oceans beyond radar network coverage. Furthermore, technologies capable of delineating lightning activity over the entire Earth, including over all oceans, have already been demonstrated. Thus, techniques for assimilating lightning data could be applied in extensive regions where radar coverage does not exist, such as the Pacific basin.

Relatively little has been done, however, to develop techniques for assimilating lightning data. One study (Alexander et al. 1999) used a single case to demonstrate an improvement in the 12-24 hour forecast of rainfall and location of convection when lightning data were assimilated along with other satellite data during model initialization. Their assimilation scheme used occasional microwave data from a low-earth-orbiting satellite to estimate the amount of rainfall per cloud-to-ground flash, used this relationship to estimate convective rainfall during all assimilation times, converted rainfall to latent heating rates, and then used latent heating to nudge the model. This assimilation significantly improved the forecast for the case study. However, because the lightning-rainfall relationship can vary by more than an order of magnitude in warm season continental storms and by several orders of magnitude for storms in different climatological regimes (e.g., pp. 225–229 of MacGorman and Rust 1998), this method of assimilating lightning data would need to be calibrated for each day and region in which it is applied.

Existing technologies for satellite-based lightning mapping systems provide a more practical and secure means for global detection of thunderstorms than CG detection networks. A limitation of satellite lightning mapping systems is that they detect both cloud flashes and cloud-to-ground flashes indiscriminately. To use satellite systems, therefore, assimilation techniques must be extended to use all types of lightning. The technique of Huo and Fiedler (1998) can be extended to all types of flashes fairly easily, but does not take advantage of the additional information that can be extracted from the lightning data.

The present study uses an approach similar to those recently developed for assimilating radar data: apply data from all types of lightning in the decision process of a forecast model's convective parameterization scheme during the assimilation period leading up to the forecast period. The focus of this assimilation research is to use lightning data to activate or deactivate subgrid-scale, deep, moist convection during the data assimilation cycle of the mesoscale model. Doing this is particularly important in situations in which past convection modifies the troposphere on scales anywhere from storm scale through synoptic scale in ways that influence the subsequent evolution of convection [for example, by moistening the boundary layer, forming surface cold pools, or modifying synoptic troughs (Stensrud 1996)]. Stensrud and Bao (1992) compared a convective parameterization trigger to a decision point in a chaotic system; an incorrect decision may have a significant adverse affect on the forecast. Rogers and Fritsch (1996) demonstrate the dramatic differences in rainfall estimates that can result from different trigger schemes.

3.2. Lightning Assimilation in COAMPS

The lightning assimilation technique was developed for and applied to the COAMPS™ mesoscale model (Hodur, 1997). The COAMPS™ was installed on the grant-supplied 750 MHZ Compaq Alpha workstation, initially run under Tru64 and later under the Alphalinux operating

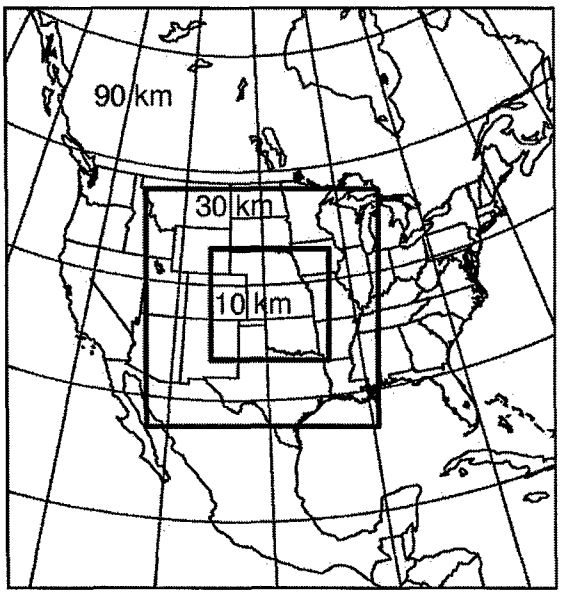

Figure 13. Model domains for the case study.

system. The model version used for this study was COAMPS™ (version 2) in research mode. Compile options for Alphalinux were supplied to COAMPS support. All forecasts were performed on the Alpha workstation platform.

All model runs in the present study employed a CONUS-scale outer grid and two finer-scale nested domains (Fig. 13) having grid spacings of 90, 30, and 10 km and minimum resolvable wavelengths of 180 km, 60 km, and 20 km, respectively. Thus, "resolvable scale" on the innermost grid implies the full representation of meso-b scale (~ 20 km – 200 km) circulations associated with a forecasted mesoscale convective system or MCS (Ziegler 1999). The innermost grid covered the STEPS program region and most of the area affected by the observed convection. The simulations all had 30 sigma-z levels, with the uppermost mass point at 31.05 km and the uppermost w-point at 34.8 km.

3.2.1. Assimilation Method

The method of lightning assimilation is similar to the technique used by Rogers et al. (2000), who used radar data to determine the occurrence of convection. Lightning observations in the present technique are similarly used to control the activation of the convective parameterization scheme (CPS), which in COAMPS is the Kain-Fritsch (KF) scheme (Kain and Fritsch 1993; Kain 2004). This method uses the forecast model's physics to estimate the effects (including latent heating) of the deep convection inferred from lightning. This differs from the method of Alexander et al. (1999) and Chang et al. (2001), who used satellite data to estimate the rainfall per cloud-to-ground flash during the assimilation period, and then used the cloud-to-ground flash rates to determine a rate of latent heat release. Their use of latent heating replaces the convective parameterization scheme during the assimilation period.

The general outline of the decision process for assimilation is shown in Figure 14. At 10-minute intervals of model time, each grid column is checked for activation of the KF scheme. If the KF scheme is not active, the model decides whether or not the KF scheme needs to be activated. An input threshold T_{flash} (with units of number of flashes per time interval per grid cell) is used to determine whether the observed lightning rate is locally high enough to infer the presence of deep convection. The lightning data could also be filtered for noise in the gridding process. (In future applications, T_{flash} could be made dependent on the grid spacing, as more noise points could be accumulated in a larger box.) If T_{flash} is met or exceeded during the assimilation period, but KF is not active, then an attempt is made to force KF to activate. Conversely, if the lightning counts are below T_{flash}, then KF may be hindered or completely prevented from activating, according to the selected level of suppression.

The KF trigger function tests successive mixed layers of air for instability. A mixed parcel is given some upward momentum to see if it can reach its level of free convection (LFC). If it can, then the KF model determines the cloud depth as the difference between the equilibrium level (EL)

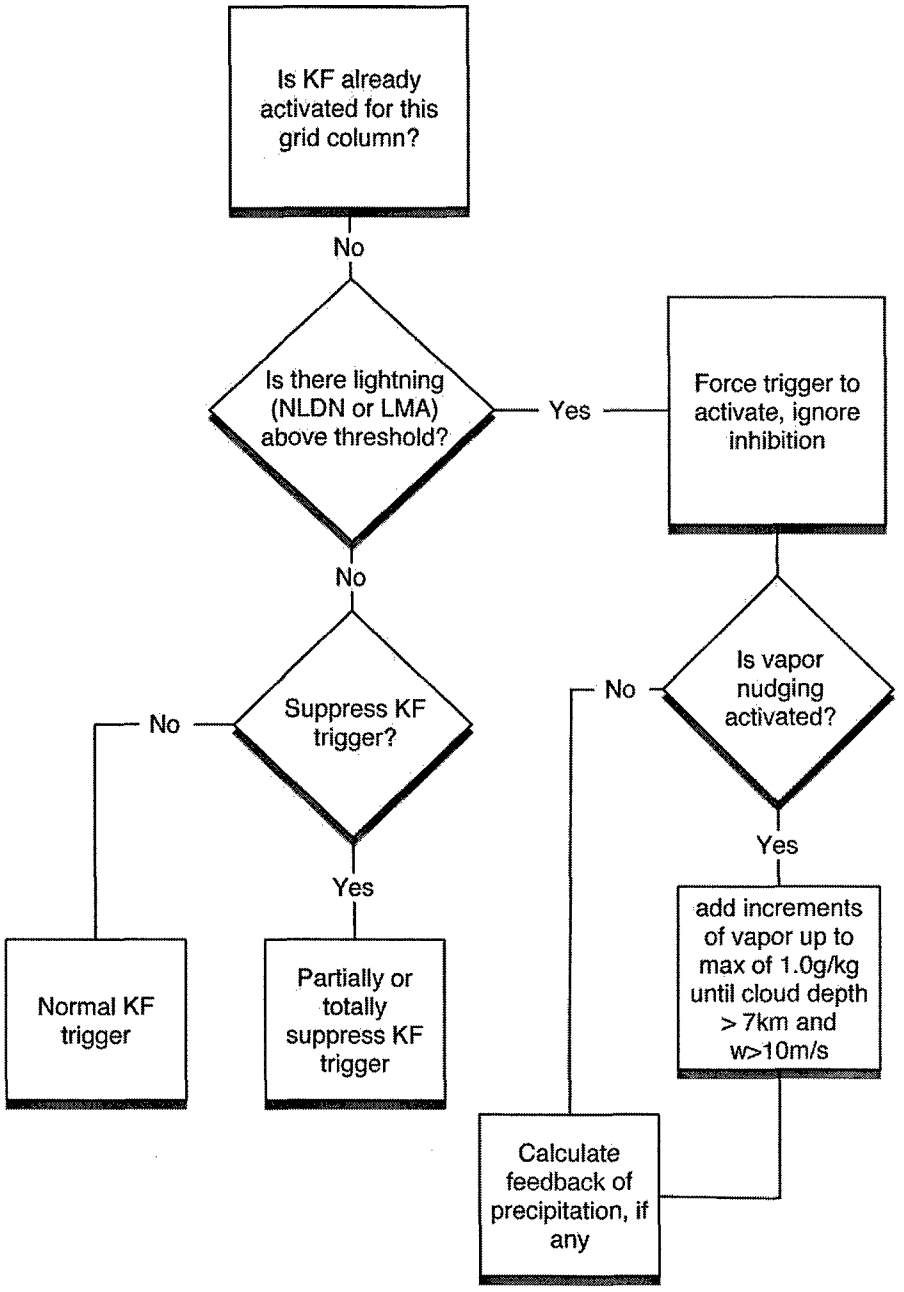

Figure 14. Decision process for lightning data assimilation and control of the Kain-Fritsch convective parameterization scheme.

and the lifting condensation level (LCL) for the most unstable parcel. (However, see the options for suppression of KF described below.)

The KF scheme uses a one-dimensional updraft mass flux cloud model to determine condensation rates, latent heating and evaporative cooling rates, and precipitation rates. The scheme includes entrainment of environmental air and detrainment to the environment. The standard scheme requires a minimum cloud depth of 4 km to produce precipitation (i.e., 4 km is the threshold for

'deep' convection). The version of KF included in COAMPS did not have the recently-added shallow (non-precipitating) convection component.

If forcing is indicated in a grid column by lightning during assimilation, the most unstable parcel in that column is found and forced to its LFC by ignoring any negative bouyancy (convective inhibition) and entrainment below the LFC. Updrafts in storms that produce lightning, however, must be strong enough to produce graupel and must extend well above the freezing level. Therefore, an option was added to increase the parcel moisture (by up to 1 g kg-1) to reach a minimum cloud depth of 7 km and peak updraft of 10 m/s. The depth and updraft thresholds were chosen as reasonable values that would be attainable on average with moisture adjustments of less than 1 g kg-1 but greater than zero. The updraft minimum was the more stringent requirement, the depth criterion being more easily attained.

For the case in which lightning is not observed in a grid column, three options were created for suppressing KF during lightning data assimilation: (s0) no suppression, (s1) partial suppression, and (s2) complete suppression. With no suppression, the KF scheme is allowed to run without interference. Choosing the second option (s1) partially suppresses the KF scheme by limiting the "boost" given to parcels by the trigger function (thereby making it harder to reach the LFC) and by restricting the updraft width of convection in the KF scheme (the width affects entrainment). By choosing the third option (s2), any grid column in which deep convection is not indicated by lightning is simply skipped by KF; the KF scheme is not allowed to run at all in that column.

A final option allowed for feedback of some convective precipitation to the resolved scaled. This option was suggested by J. Kain (personal communication, 2004) as a possible means to generate stronger cold pools though evaporation in the resolved-scale microphysics. Feedback is enabled during assimilation only where lightning was observed. Occasionally, precipitation feedback causes an imbalance in the KF moisture budget above the tolerance limit in a particular grid column. In those cases, the feedback fraction is automatically reduced until the imbalance is reduced below the limit. It was noticed that advection and mixing of snow and rain were disabled by default, even at scales where the KF scheme would be active (i.e., where dx is greater than dxmeso in the COAMPS code), so advection and mixing were activated during subsequent runs with precipitation feedback. In the future, it is recommended that advection and mixing of snow and rain be enabled as the default, to avoid artifacts in the model physics.

3.2.2. Data Sources

Lightning observations were taken from two platforms: (1) the National Lightning Detection Network (NLDN), which covers the 48 contiguous states, and (2) the Lighting Mapping Array (LMA), which operated in northwestern Kansas and northeastern Colorado during the STEPS field program in the summer of 2000. (STEPS = Severe Thunderstorm Electrification and Precipitation Study.) The NLDN detected only cloud-to-ground (CG) strikes. The LMA detected very high frequency (VHF) radio emissions from both intracloud (IC) and cloud-to-ground (CG) lightning flashes, but did not automatically distinguish between the two, nor did it automatically group source points into flash events. Each lightning flash may generate 10's to 1000's of source points in the LMA data.

The NLDN and the LMA provide point data that must be gridded for ingest by COAMPS in the present assimilation scheme. The altitude information in the LMA data are ignored at present, though the full 3-D could be utilized in a future follow-on study by using a modified assimilation function (e.g., to estimate cloud depth). The two lightning data sources are each gridded into separate arrays that match the domains of the nested COAMPS grid configuration (e.g., as in Fig. 13

for the present study). Data are accumulated for 15 minute periods over a full 12 hour update cycle, and each detected lightning point (from either the NLDN or LMA) simply increments the count in the grid box in which it falls. (For example, the data file "cgdat1.2000072112" contains NLDN data on grid 1 for the 12 hour period beginning at 12 UTC on 21 July 2000.) Other integration periods may be chosen, but the choice governs both the temporal resolution and spatial continuity of the gridded data. Fifteen minutes was chosen because it gave good temporal resolution while providing enough samples to alleviate the patchiness that can result from gridding point data.

A 'look-ahead' parameter in the assimilation routine determines how far into the future to look for the occurrence of lightning. For the present study, a look-ahead parameter of 30 minutes was used, so that two 15-minute time periods would be aggregated and used for controlling the KF routine. (A typical time scale for KF convection is 20 to 30 minutes.) For NLDN data, the threshold T_{flash} to force KF was set at 1 strike per grid box during the look-ahead period. In the future, it may be desirable to use a threshold of 2 to avoid occasional activation of KF by spurious noise. For LMA data, T_{flash} was set at 10 points per grid box per look-ahead period, which was sufficient for removing noise points. (Noise can also be removed by evaluating lightning data at the gridding stage, but this was not done in the present study.)

The NLDN has the advantage of large area coverage but has the shortcoming of detecting only CG lightning, which is a small fraction of all lightning (averaging roughly 25% nationally, but 10-15% over the inner grid used in this study). The coverage of the NLDN makes it a good platform for determining the occurrence of deep electrified convection, especially of long-lived large systems that produce many CG flashes. The LMA, on the other hand, detects total lightning (10s-100s of points per individual flash), but covers only out to roughly 200 km from the network center. (In the STEPS field program, the network center was in far northwestern Kansas.)

An example of NLDN and LMA data for a 15 minute period during the MCS event to be described later in this report illustrates typical differences in the detail of the ongoing convection available from each source, as well as the spatial coverage of the two networks (Fig. 15). The LMA data have far greater detail, giving a better picture of the electrical intensity, cellular structure, and coverage of individual storms within the LMA detection range (eastern Colorado, western Kansas, and southwestern Nebraska). The NLDN indicated storms in central Kansas and northern New Mexico that were out of LMA coverage. Storms in the high plains region of the U.S. tend to have a lower percentage of CG flashes than the U.S. average (e.g., Boccippio et al. 2001), so the difference shown in the figure may be greater than typical of other regions. Since the LMA detects total lightning, it can more accurately determine the timing of initial strong electrification than the NLDN, because the first flashes in storms are usually IC discharges.

3.2.3. Upgrades of the KF parameterization code in COAMPS

Two straightforward upgrades of the numerical code responsible for implementing the KF parameterization in COAMPS are described in the present section. These code upgrades are believed to be important enough to bring to the attention of ONR, as they relate to efficient use of CPU cycles and memory by the COAMPS. Other updates to the KF scheme were considered (e.g., the addition of the presently available shallow convection parameterization), and an initial attempt was made to incorporate them into the code via compiler directives. It was decided that it was beyond the scope of the project to spend the time to debug the new features, however, so these other updates were not fully implemented and were not used.

Early model experiments would sometimes stop due to a floating point exception occurring in the KF parameterization code. It turned out that the cause of the error was the following simplified

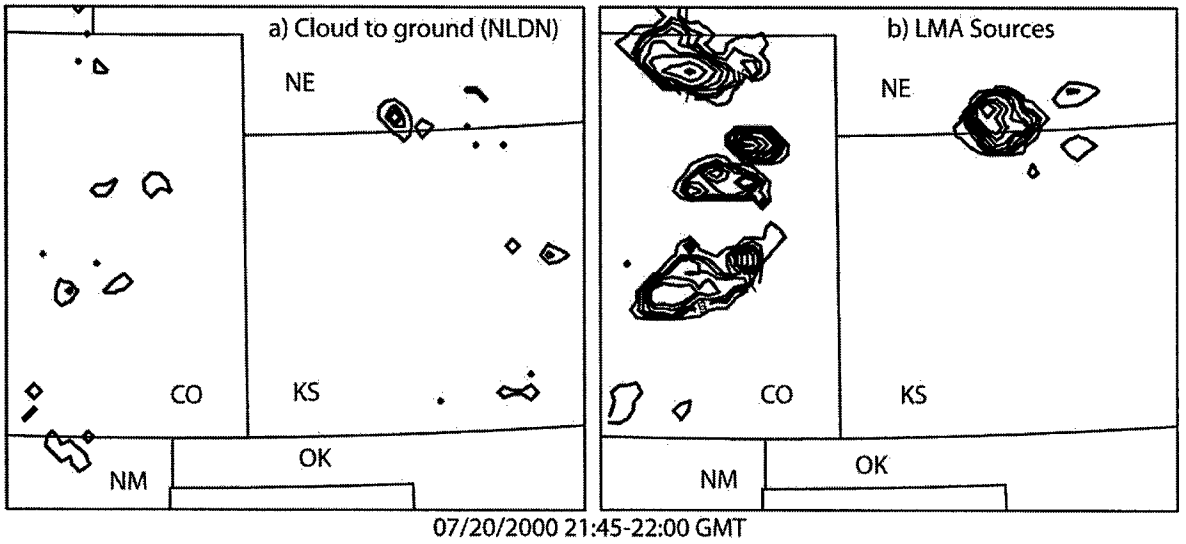

Figure 15. Lightning data for the 15 minute period starting at 21:45 UTC on 7 July 2000. (a) Cloud-to-ground detections by the NLDN. (b) VHF source points from the STEPS-LMA. Contour levels are 1, 5, 10, 20, 50, 100, 250, 500, and 1000. (The lowest level in (a) is 0.8 to make single flashes visible.)

code line calculation:

```
eqfrc(nk1) = (thtes(nk1)-theteu(nk1))/(thetee(nk1)-theteu(nk1))
```

where the denominator could be very small or zero and cause an overflow error. (This calculation remains unchanged in COAMPS version 3.) COAMPS support recommended compiling COAMPS with double precision floating point variables (S. Chen, personal communication). The use of double precision hides this problem by fairly well guaranteeing that the divisor is never zero, but it also results in a doubling of memory and memory bandwidth requirements. J. Kain (personal communication, 2004) recommended restoring the standard version of calculating eqfrc, which, although more computationally expensive, is more accurate and avoids the need for double precision. The savings in memory and bandwidth more than compensated for the extra computation involved in the longer calculation. The shortcut version remains available through a precompiler flag (#ifdef conditional). All forecasts in the results used the long version of the eqfrc calculation.

Another small issue was a code bug in logic to determine whether the KF routine should be called. The intent of the release code was to call the KF driver routine every third step on the coarse grid with the following statement:

```
If (mod(iter1-ncldck/2,ncldck).eq.0) then
```

Execution of the latter statement had the effect of calling the KF driver on every iteration of nested grids within the coarse time step; this caused repeated calculations of static stability in all grid columns and unnecessarily increased CPU time. (The variable `iter1` is the iteration number of the coarse grid, so when the condition is met, the KF driver will be called for the coarse grid and for every iteration of the nested grids; this can produce many calls for multiple nest levels.) The

conditional statement was changed to call the KF driver approximately every 10 minutes on each grid by using the following statement:

```
If (mod(itnn,Int(tstn)).eq.0 .or. itnn.eq.1) then
```

where itnn is the time step number for the current grid and Int(tstn) is the number of time steps (truncated to the integer value) which the model takes on that grid within 10 minutes; itnn is the value of the array it(nn) passed to the routine from module coamm.F. The original version of the code resulted in unnecessarily frequent calls of subroutine kfdrive. It appears that the base code has not changed in COAMPS version 3, so this bug still exists.

3.3. Case Study

The lightning assimilation method was tested with a case from July 2000 in the U.S. central plains. The STEPS field program operated in the region of western Kansas, eastern Colorado, and southwest Nebraska, and a lightning mapping array (LMA) covered approximately a 200-km radius centered near the Kansas-Colorado border (Fig. 5). Widespread convection occurred on each of successive days (20 to 22 July 2000). On each day, convection initiated in Colorado and/or Nebraska and developed into convective systems that traversed Kansas into Oklahoma, Missouri and Arkansas. Convection also developed in a similar manner on 19 July, but was not as extensive or long-lived.

Since the major objective of the study was to improve the forecast initial condition through the generation of cold outflow boundaries from previous convection, a 24 hour assimilation spin-up period was run from 00 UTC on 20 July through 00 UTC on 21 July 2000. On 20 July, deep convection had initiated in eastern Colorado by 00 UTC, and squall lines had developed in Nebraska and Kansas by 06 UTC. By 12 UTC, a large system covered southeastern Kansas and parts of Oklahoma and Missouri. The system moved into Missouri and Arkansas by 16 UTC, and new storms began forming in Colorado and Kansas by 20 UTC. A vigorous system was in place in northeastern Colorado by 00 UTC 21 July, with convection also evident in southern Colorado and north-central Kansas/south-central Nebraska (Fig. 16). The spin-up period thus had both earlier convection and new, ongoing convection and a combination of old and new outflow boundaries (Fig. 16).

3.3.1. Model Setup and Initialization

The Kain-Fritsch CPS was enabled on all grids, and COAMPS was initiated at 00 UTC on 20 July 2000 ("cold" start) from analyses, with boundary conditions from NOGAPS. The 24-hr spin-up period was performed for all forecasts, including a 12-hourly ingest of atmospheric observations via the built-in multivariate optimal interpolation (MVOI). For all experiments other than the control run, lightning data assimilation options were enabled during the spin-up period. For lightning cases, assimilation of NLDN data was always enabled on the outermost grid. Suppression of KF was never chosen for the outermost grid, because it extended beyond the range of the NLDN. The middle grid, however, always had the same KF suppression option as the innermost grid. Due to the limited spatial coverage of the LMA, its data were assimilated only on the innermost grid, always with NLDN data being assimilated, too. A 12-hr pure forecast was then initiated from warm-start conditions at 00 UTC on 21 July 2000.

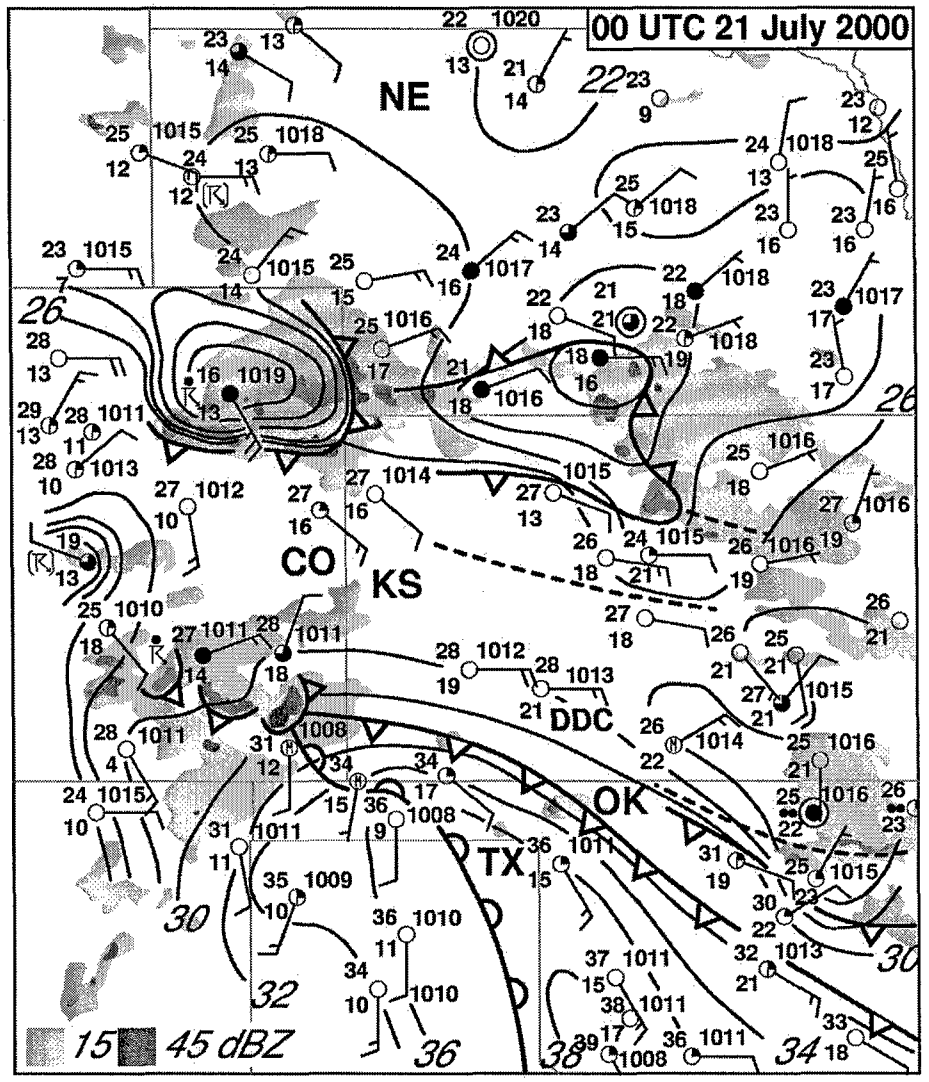

Figure 16. Surface analysis at 00 UTC on 21 July 2000, the starting time for the forecast period. Conventional station model format includes temperature (°C) over dewpoint (°C), mean sea level pressure (mb) at upper right, and wind barb (full barb = 5 m s^{-1}, half barb = 2.5 m s^{-1}). Instantaneous base radar reflectivity is shown by gray fill. The site of Dodge City sounding discussed in the text is indicated by "DDC."

3.3.2. Results during Assimilation

3.3.2.1. Precipitation

Lightning data assimilation substantially improved the location and amount of precipitation during the spin-up period. Figures 17 and 18 display the precipitation accumulation during the period 06 to 12 UTC (20 July 2000) as reported by rain gauges and from different forecast experiments. The control run (Fig. 17b) had the least (and so worst) rainfall amounts, although the greatest values being placed accurately with the larger observed rainfall values in Kansas suggests some skill on the

part of the base model. The lightning assimilation cases produced more rain in Kansas as well as capturing some convection in southeastern Nebraska. Water vapor nudging was able to substantially enhance the amounts of precipitation (compare Figs. 18b and 18c), but the rainfall was still less than was observed. The quantitative precipitation estimate during the lightning assimilation period was

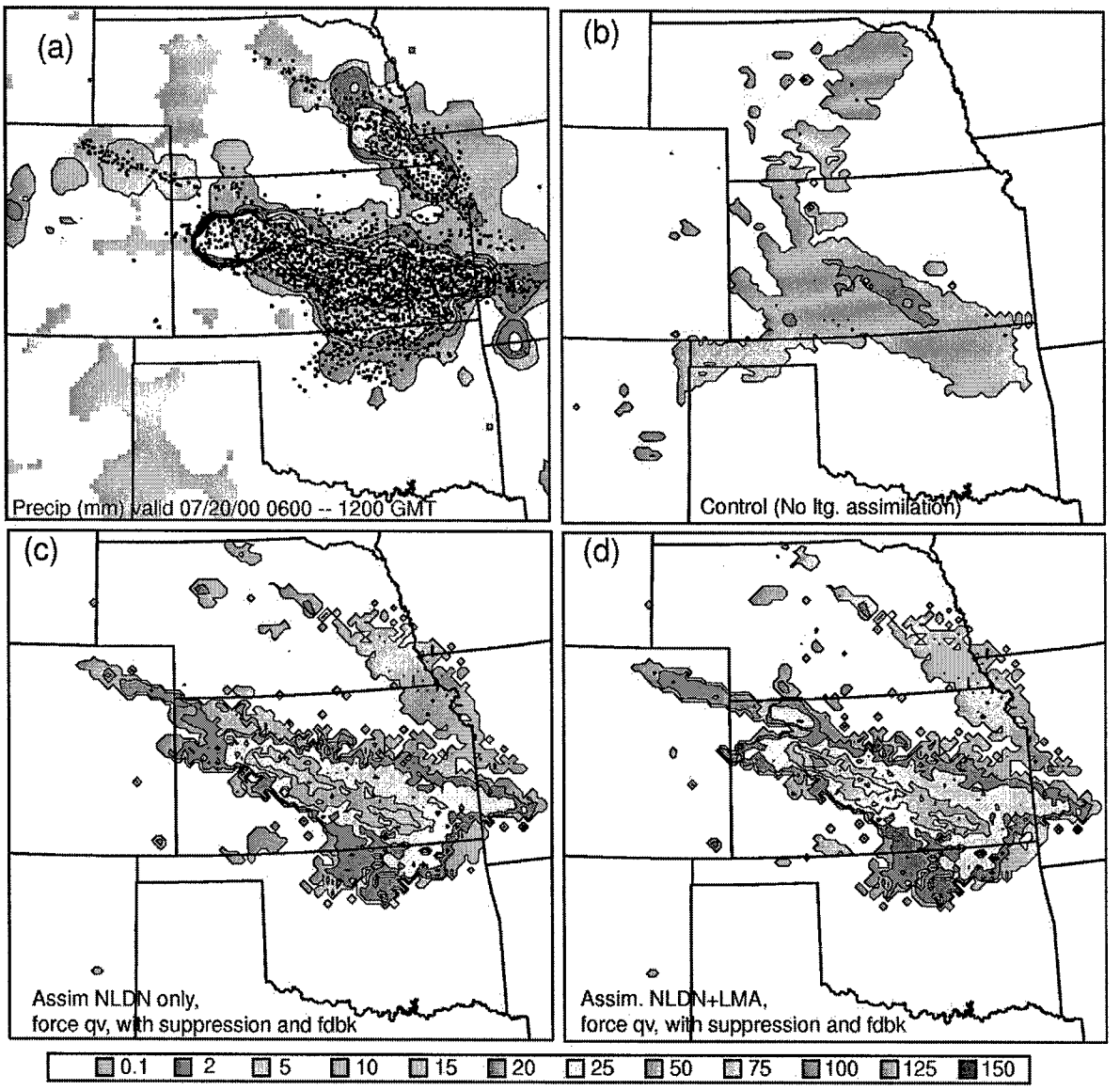

Figure 17. Observed and modeled total precipitation (mm) for a 6-hr period starting 07/20/2000 06 GMT during the spin-up period. a) Rain gauge data with sampled NLDN strikes. (The first and 30th strikes are plotted in each 10 km grid box.) Gray-filled areas indicate data voids. b) Pure forecast (no lightning assimilation). c) With assimilation of CG lightning from NLDN by using moisture forcing to aid triggering when lightning was present and using full suppression when lightning was absent. d) With assimilation of both CG and total (LMA) lightning by using moisture forcing in the presence of lightning, full suppression without lightning, and 25% feedback of KF precipitation.

up to approximately 40 % of observed precipitation amounts. This supports the conclusion that forcing subgrid convection when lightning is present maintains much more realistic intensity and coverage of convection.

Though assimilating NLDN ground strike data alone provided considerable improvement (Fig. 17c), some further improvement occurred when LMA total lightning data were assimilated with NLDN ground strike data (Fig. 17d). The addition of LMA data enhanced rainfall in western Kansas,

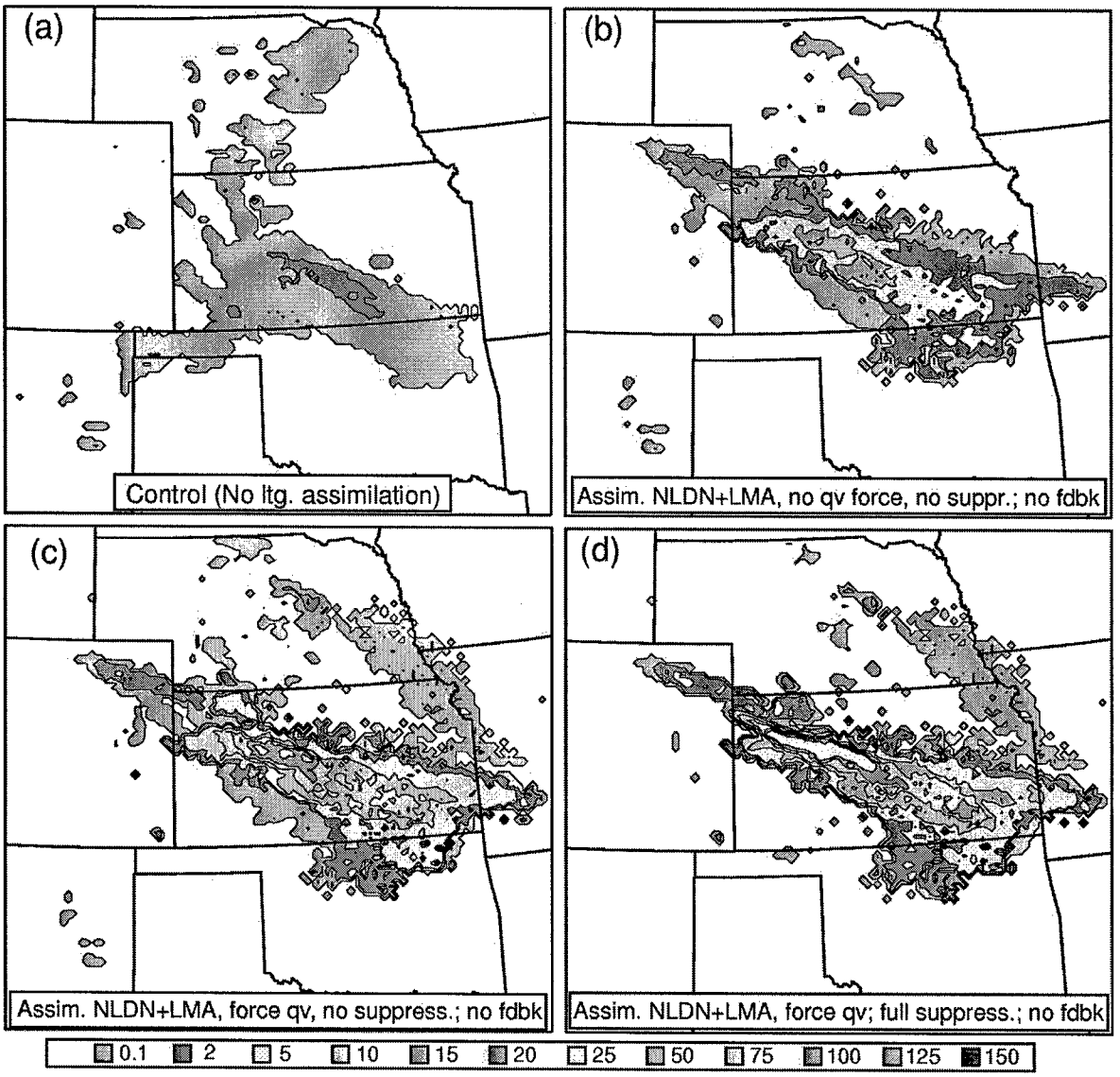

Figure 18. Modeled total precipitation (mm) for a 6-hr period starting 07/20/2000 06 GMT during the spin-up period. These simulations have no precipitation feedback from the CPS to the resolved scale. a) as in Figure 4b (control run). b) Normal KF trigger with forcing from lightning assimilation. c) as for (b) adding nudging of boundary-layer moisture. d) as for (c) but suppresses the KF trigger where no lightning occurred (no precipitation feedback). The region of heaviest rainfall in (d) has a substantial resolved-scale contribution.

though perhaps a little too much in the extreme northwestern part of the state.

Suppressing convection from the KF scheme where no lightning was observed helped to remove the spurious precipitation seen in the control forecast in Nebraska and in the Oklahoma panhandle region. The experiments that did not actively suppress KF were also able to reduce the frequency of spurious convection (Fig. 18b,c) that was present in the pure forecast mode, possibly because assimilation improved the boundary conditions provided from the outer grids.

3.3.2.2. Effects on forecast initial conditions

A particular interest of this research is the generation of mesoscale boundaries by convective outflows. Surface and WSR-88D radar mosaic observations at 00 UTC on 21 July indicate a strong, cold outflow forced by convection in northeastern Colorado, as well as boundaries in southeastern Colorado, north-central Kansas, and across Oklahoma (Fig. 16). The surface temperature fields from four model experiments are shown for comparison in Figure 19. (A cold-start analysis had an obvious cold bias, and is not shown.) The control case (Fig. 19a) did not generate the observed convection in northeastern Colorado during the spin-up period and, therefore, failed to build the observed surface cold outflow. A clear difference from the control run is seen in the experiments with lightning assimilation (Figs. 19b,c,d): a convectively-generated cold pool is evident in northeastern Colorado as seen in the surface analysis. The case with assimilation of NLDN data only (Fig. 19b) developed a cold pool where convection was observed in northeastern Colorado, but it is weaker than when the same options were used with total lightning assimilation (NLDN plus LMA; Fig. 19d). This is a result of the sparseness of the NLDN ground strikes compared to the LMA total lightning data (seen in Fig. 15).

In the two examples with total lightning assimilation, a stronger thermal gradient around the cold pool can be seen in the experiment in which spurious convection was actively suppressed (compare Figs. 19c and 19d). It should be noted that for Fig. 19d, the assimilation forecast actually had a low temperature of 18°C in the cold pool (compared with 16°C in the surface observations and 20.76°C after the MVOI adjustment). The MVOI procedure warmed the cold pool minimum by 2.8°C, but did preserve the thermal gradient. We used the default option in which the MVOI adjustments from the coarse grid were interpolated to the inner grids (loimf=.false.). A test with loimf=.true. resulted in less warming (1°C) of the cold pool, but it also appeared to cause a general cold bias on the innermost grid. The MVOI issue needs more study before any conclusions can be made.

Soundings at Dodge City, KS, (DDC) also illustrate differences in the initial conditions generated by the control and assimilation experiments. The observed National Weather Service sounding from DDC at 00 UTC on 21 July 2000 is plotted in Figure 20 (the sounding location is shown in Fig. 16). Model-generated soundings at the DDC location are shown in Figure 21 from before and after the MVOI analysis. The control run sounding was saturated from 300 mb up to about 175 mb due to anvil outflow of spurious convection to the southwest of DDC. On the other hand, the sounding from the lightning assimilation case is drier and more unstable above the moist boundary layer in agreement with the observed sounding (i.e., it does not exhibit contamination by convection) and, except for the near-surface winds, compares more favorably with the observed sounding. The homogeneously mixed elevated residual layer (ERL) above the moist boundary layer in the lightning assimilation sounding probably would have been rather more mixed along a moist virtual adiabat, in agreement with the observed profile under the action of a cumulus field, had the shallow cumulus convection parameterization, mentioned in section 3.2.1, been added to COAMPS and activated in the present model runs.

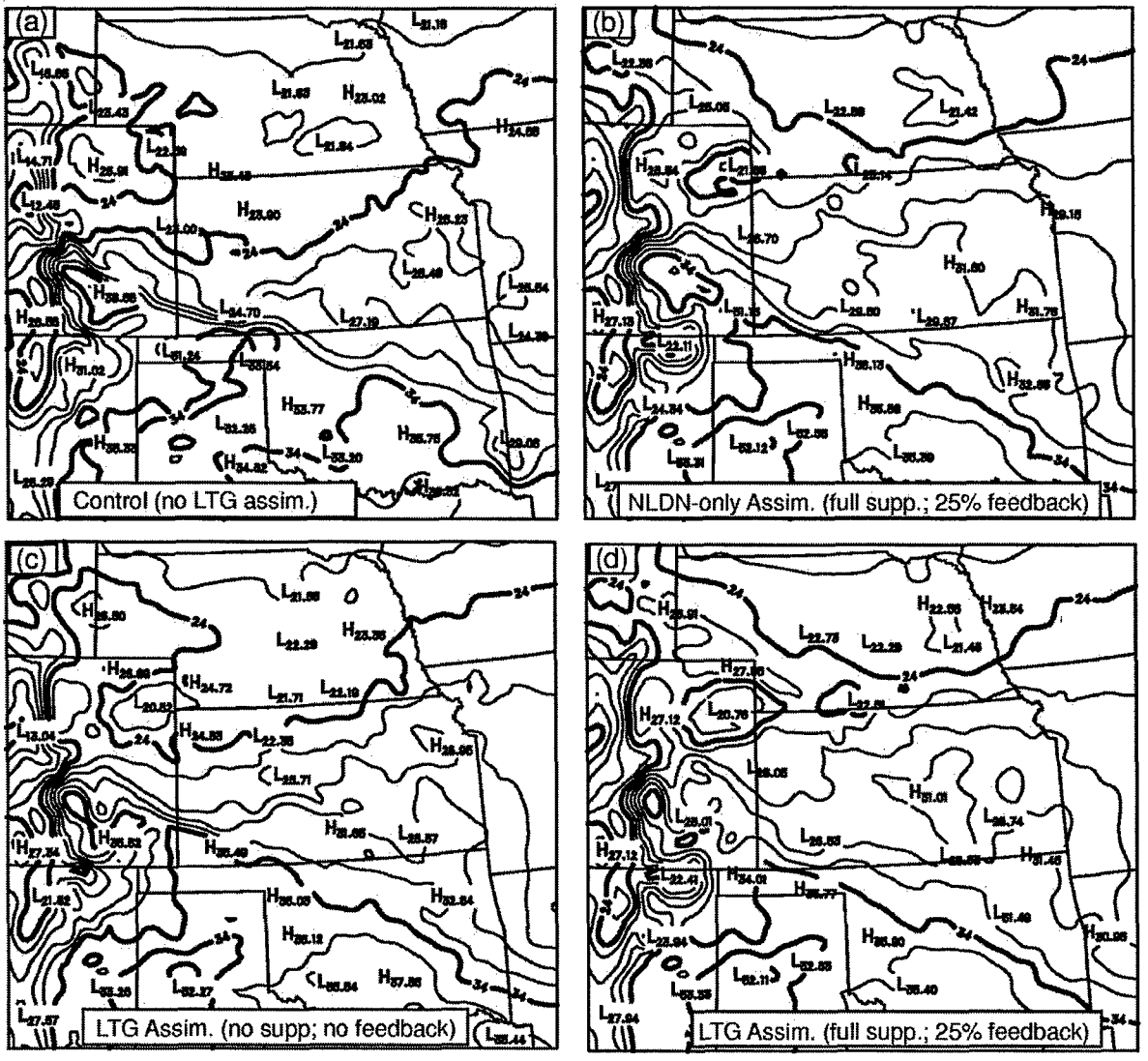

Figure 19: Air temperature (2 m) at 00 UTC on 21 July 2000, the beginning of the forecast period. (a) Warm start with 24-hr spin-up, 12-hourly data update cycle. (b) 24-hr assimilation of NLDN only with full suppression and 25% feedback of precipitation from KF to the resolved scale. (c) 24-hr assimilation of all lightning (NLDN and LMA) data to force convection (no suppression of KF nor feedback of precipitation). (d) As for b but with assimilation of both NLDN and LMA data.

Examination of ground layer conditions in the model output data (not shown) indicate that increased convective and total precipitation caused a significant increase in soil moisture in areas of antecedent convection. Given the demonstrated ability of assimilating lightning data to improve quantitative precipitation estimates during the assimilation period, soil moisture availability is then theoretically more reliable in areas which had received heavy precipitation. The spatial soil moisture availability field is highly relevant to the determination of mesoscale surface layer fluxes (Marshall et al. 2003). Local soil moisture variations due to factors such as previous convective precipitation may assist in forcing boundary layer evolution and convective initiation during subsequent diurnal cycles

(e.g., Ziegler et al. 1995, Ziegler et al. 1997).

3.3.3. Results: Forecast

A main hypothesis for this study was that correctly locating soil moisture and outflow boundaries for the initial condition should improve model forecasts by improving the placement of physical mechanisms for triggering convection. Lightning data assimilation was successful in reproducing observed cold outflow, so the remaining test is whether forecast skill was improved.

Observed and forecast rainfall accumulations for 6-hr forecast periods are shown in Figure 22 (00 to 06 UTC on 21 July 2000) and Figure 23 (06 to 12 UTC). The larger observed rainfall accumulations from 00 to 06 UTC stretched from east-central Colorado and northwestern Kansas to south-central Kansas (Fig. 22a). Compared with the

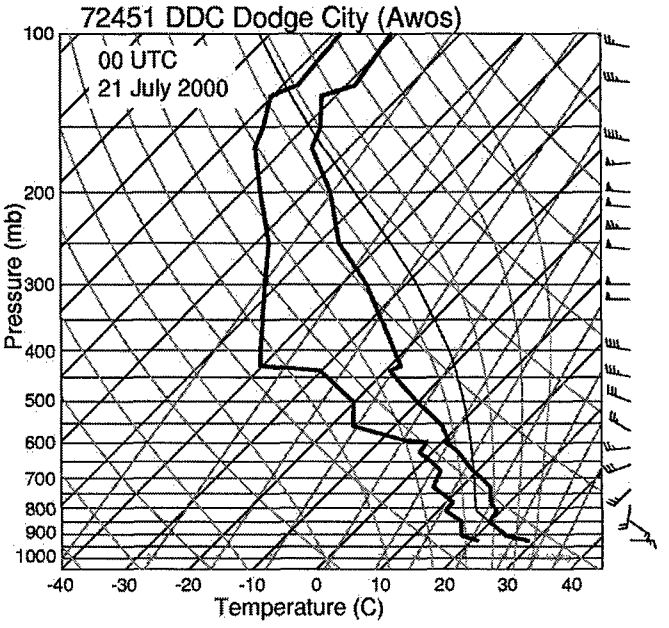

Figure 20: National Weather Service sounding for Dodge City, KS, at 00 UTC on 21 July 2000.

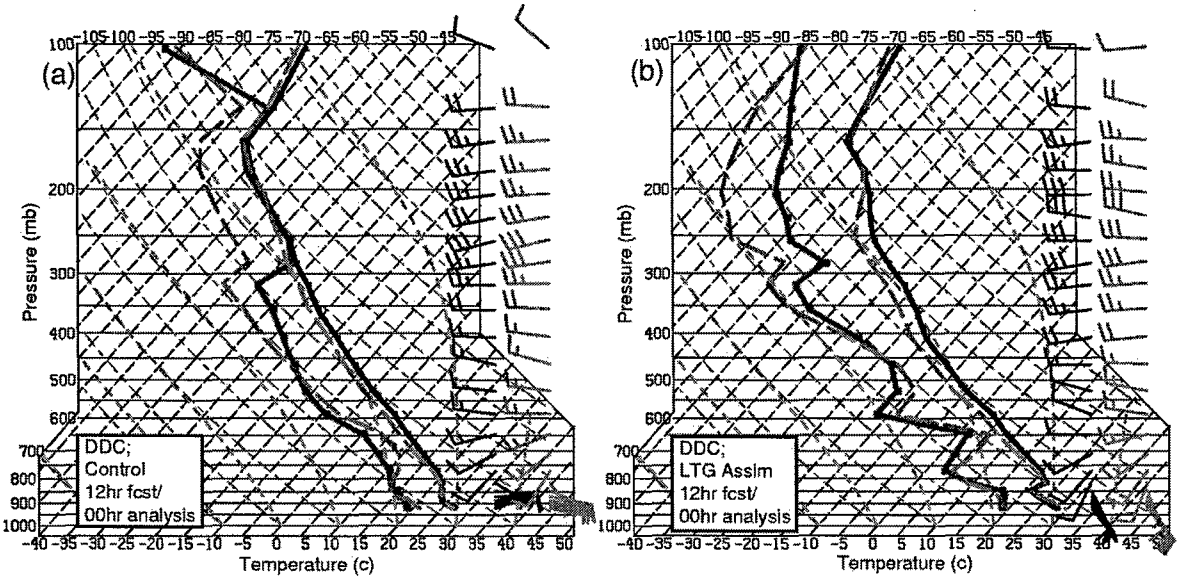

Figure 21: Model soundings for Dodge City, KS, at 00 UTC on 21 July 2000. Red and black curves show dewpoint and potential temperature, respectively, of the 12-hr forecast. Long dashed curves are the adjusted values after the initialization of the next forecast cycle. Black wind barbs are from the forecast, gray barbs are from the subsequent analysis adjustment. (a) Control run (no lightning assimilation). (b) Simulation with assimilation of lightning (NLDN and LMA), full suppression, and 25% feedback of precipitation from the KF scheme to the resolved scale.

control forecast, the forecasts based on lightning assimilation (Fig. 22b,c) produced a more accurate pattern of the larger rainfall accumulations in this region and produced more rainfall, closer to the observed values. The assimilation-based forecast that did not suppress the KF scheme (Fig. 22c) had less spurious convection in Nebraska than the other experimental forecast, but it also had a greater overestimate of rainfall in northeastern Kansas. In the second six-hour period of the forecast, from 06 to 12 UTC, the heaviest observed accumulations had moved into Oklahoma, and relatively large values extended into south-central and southeastern Kansas (Fig. 23a). By this period, the pattern and amount of rainfall accumulations in Kansas from the experimental forecasts were converging on the pattern from the control forecast, but in Oklahoma, the pattern and amounts of rainfall from the experimental forecasts were still more accurate than those from the control run. Though the experimental forecasts were at least somewhat better than the control forecast throughout the period, note that the larger values of rainfall accumulation in the experimental forecasts, dominated by subgrid-scale convective precipitation, became a smaller fraction of the observed accumulations with time—from roughly 20% of the larger observed accumulations at 00-06 UTC to roughly 10% of the larger observed accumulations at 06-12 UTC.

This decrease in the forecasted rainfall accumulation relative to observations can be understood better by focusing on the early hours of the 00-06 UTC forecast period. A comparison of the hourly evolution of the observed radar reflectivity and cold pools with that of the forecasted convective rainfall and the associated cold pool boundaries shows that assimilation of lightning data into the initial conditions did, in fact, improve the first several hours of the forecast mesoscale evolution (Fig. 24).

The observations show that a convective line from northeastern Colorado (cold pool #1 in Figs. 24a,d) propagated roughly toward the southeast, with other storm elements going eastward just north and south of the Kansas-Nebraska border. The observed storms in southeast Colorado (cold pool #2) weakened slightly and moved to the east over the two hour period. At 02 UTC, the radar showed a hint of an outflow boundary heading southward though east-central Colorado. Cold pool #3, associated with other forecast convection in northeast New Mexico, could not be validated, because of sparse surface observations and radar blockage by terrain.

The control forecast (Fig. 24c,f) failed to generate any significant convection in northwestern Kansas or along the Kansas-Nebraska border, but produced convection along a temperature gradient that arched through southeastern Colorado and extended farther into southwestern Kansas than observed (Fig. 19b). In the experimental forecast (Fig. 24b,e), on the other hand, propagation of the two outflow boundaries (#1 and #2) was similar to the observed behavior. [This improvement is analogous to the improvement found by Pereira Fo. et al. (1999) when they assimilated rainfall rate data to initialize a mesoscale forecast model.] During the first hour, convection was triggered by the assimilation-produced cold pools in eastern Colorado, southwestern Nebraska, and northwestern Kansas, much as was observed. A third outflow (#3) was evident in northeastern New Mexico, but was not obvious in the radar data, probably due to a combination of terrain blockage and longer range from the proximate WSR-88D radar. The main convective line produced in northeast Colorado by the assimilation propagated southward instead of southeastward, but nevertheless demonstrated some skill in the assimilation-based forecast, compared to no skill in forecasting this convection in the control run. The convection in southeastern Colorado was also better in the experimental forecast than in the control run, in terms of placement, rainfall amounts, and the extent of propagation eastward into Kansas. However, the experimental forecast also had some spurious convection in Nebraska and southwestern Iowa.

The convection in the second hour of the experimental forecast weakened relative to the observed convection, because the cold pools spread out and were not sufficiently sustained by new convection in the forecast period. This weakening is particularly noticeable in the decreasing area of forecasted larger rainfall accumulations (compare Figs. 22b and e), whereas the observed area of larger reflectivity was relatively unchanged (compare Figs. 22a and b). Much of this weakening can probably be attributed to the already-discussed tendency for all activated subgrid-scale convection

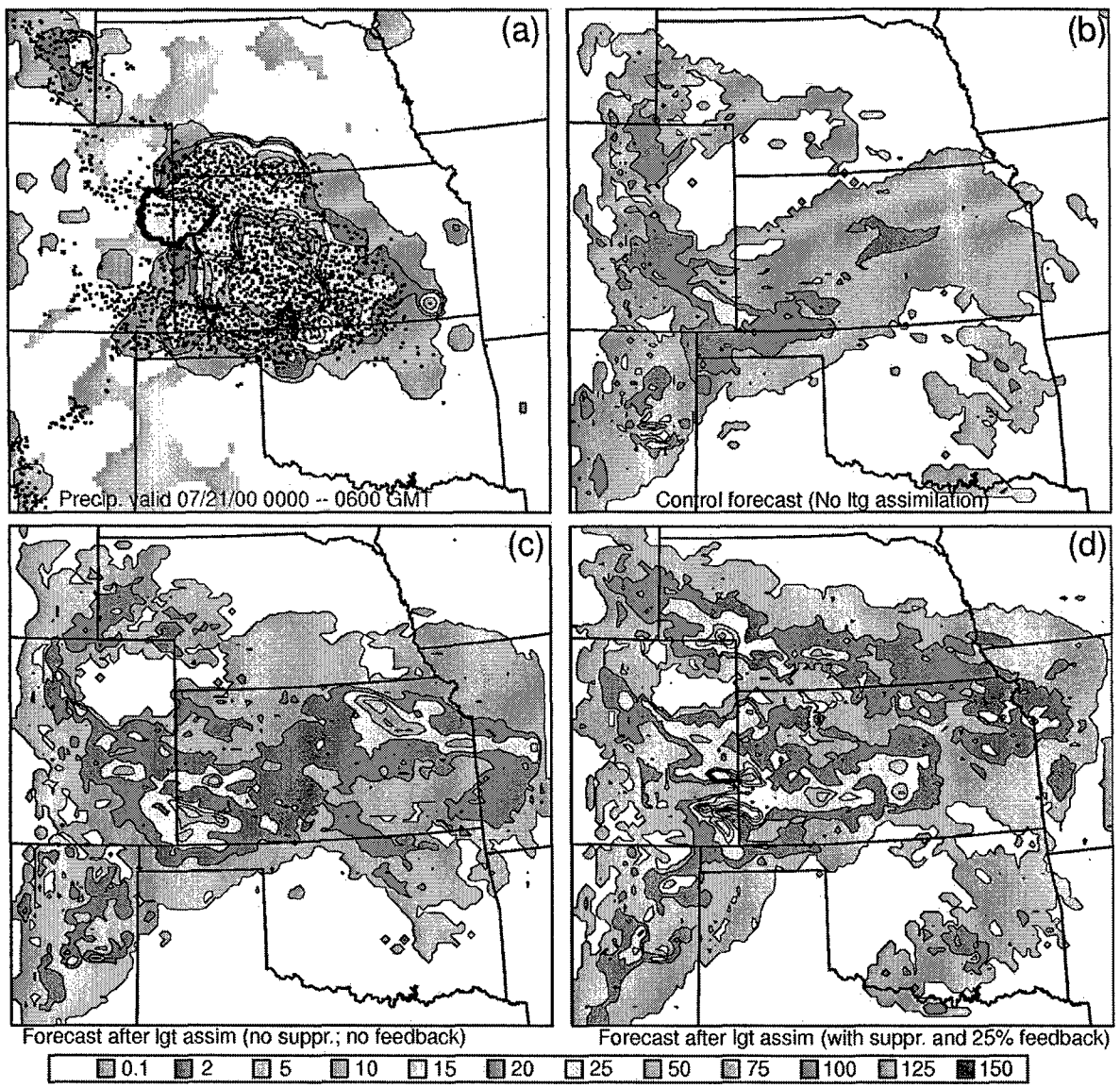

Figure 22. Observed and forecast total precipitation (mm) for the 0–6 hr period starting 07/21/2000 00 GMT. (a) Rain gauge data with sampled NLDN strikes. (The first and 30th strikes are plotted in each 10 km grid box.) Gray-filled areas indicate data voids. (b) Pure forecast from standard warm start (no lightning assimilation). (c) Forecast from initialization with assimilation of NLDN and LMA data, moisture forcing, and no suppression nor feedback. (d) Forecast from initialization with assimilation of both CG and total (LMA) lightning, moisture forcing, and full suppression and 25% feedback.

in the model to produce too little rainfall. As discussed in the last section, rainfall accumulations were only 40% of observed values, even when the convection was being nudged continually by observations, and the underestimating of rainfall increased with time in the forecast period, as shown in Figs. 22 and 23. Under-forecasting precipitation weakens the resulting cold pool, and so also weakens the subsequent triggering of convection by the cold pool. This feeds back tends, in turn, to further reduce the rainfall produced by the newly triggered convection.

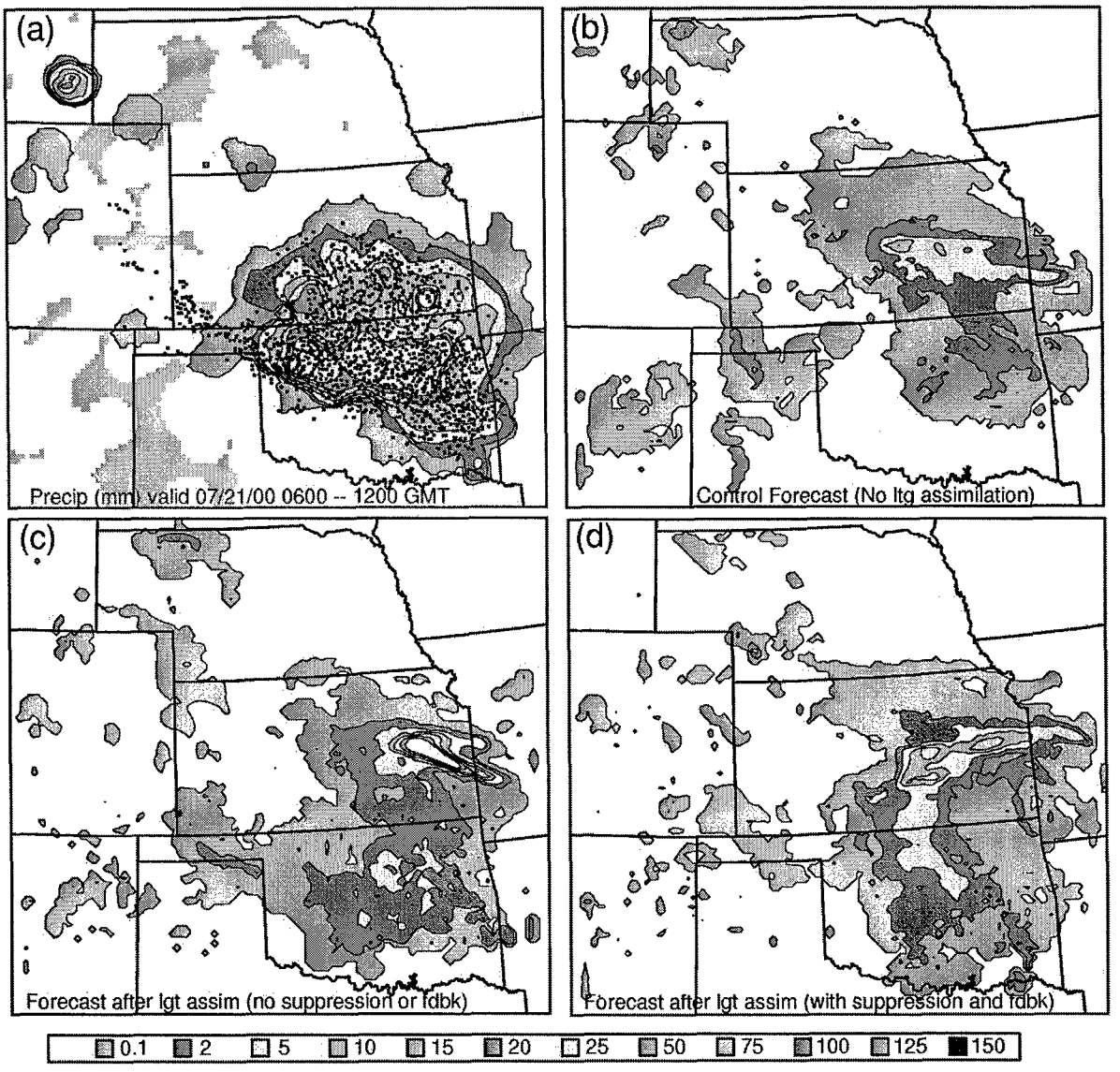

Figure 23. Observed and forecast total precipitation (mm) for the 6–12 hr period starting 07/21/2000 06 GMT. (a) Rain gauge data with sampled NLDN strikes. (The first and 30th strikes are plotted in each 10 km grid box.) Gray-filled areas indicate data voids. (b) Pure forecast from standard warm start (no lightning assimilation). (c) Forecast from initialization with assimilation of NLDN and LMA data, moisture forcing, and no suppression nor feedback. (d) Forecast from initialization with assimilation of both CG and total (LMA) lightning, moisture forcing, and full suppression and 25% feedback.

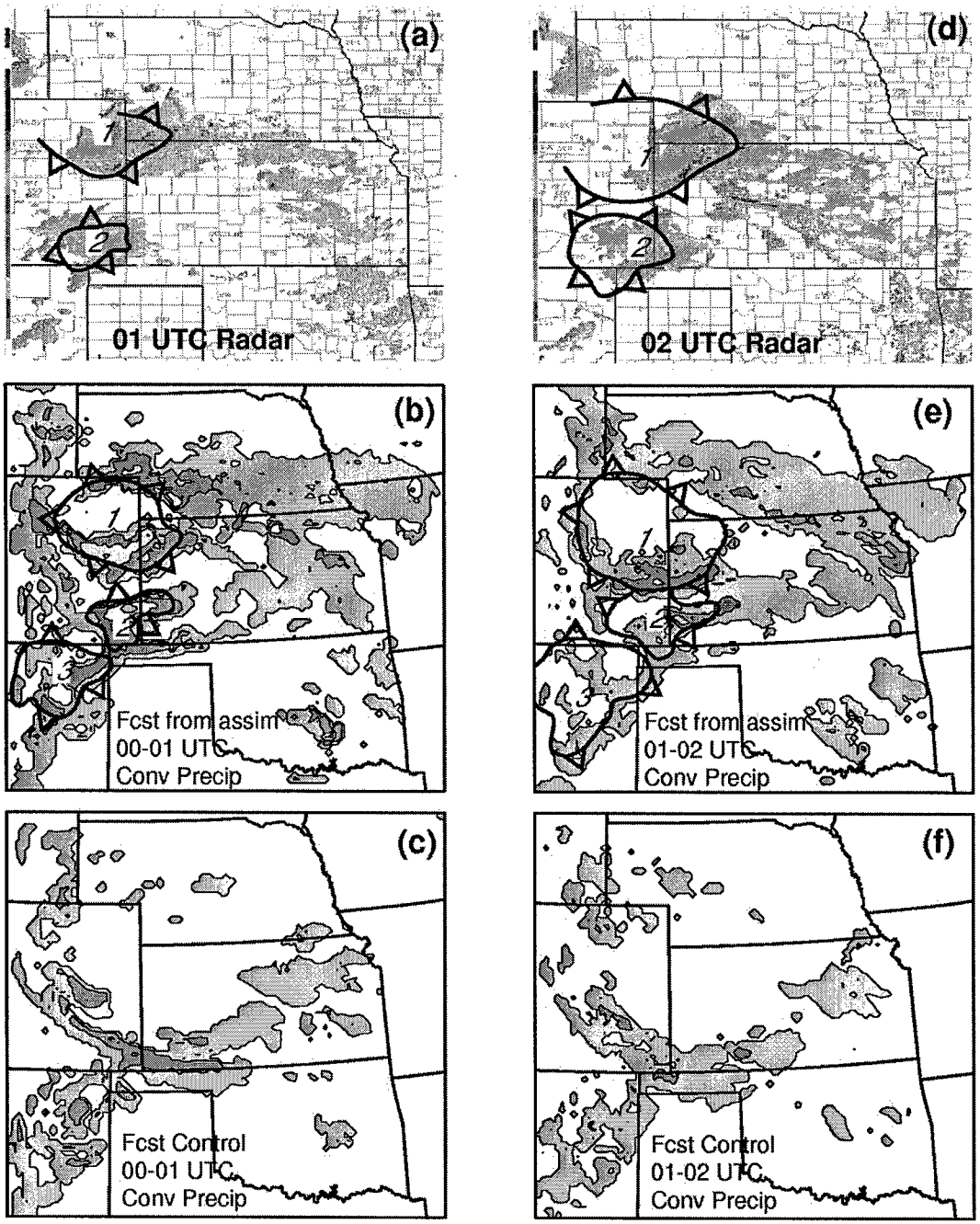

Figure 24. Radar composites and convective precipitation forecasts on 21 July 2000. (a) Radar composite at 01 UTC. (b) 00-01 hour precipitation forecast from initial condition generated by assimilation of both CG and total (LMA) lightning, moisture forcing, and full suppression and 25% feedback. (c) 00-01 hour control forecast from standard warm start (no lightning assimilation). (d, e, f) As for (a, b, c) but for 02 (01-02) UTC. Observed and forecast cold pool boundaries are overlaid, the latter determined from the forecast surface temperature field associated with convective rainfall cores. For reference, reflectivity at 00 UTC was depicted in Fig. 16.

3.4. Conclusions of the Lightning Assimilation Study

Assimilating lightning data to control parameterized convection in the spin-up cycle of a forecast model has been shown to be promising in improving the effects of prior convection on the initial condition of the forecast period. The most important effects of more accurate prior convective precipitation on the initial condition include more accurate representation of cold pools in the boundary layer, an absence of convective contamination of the environment where convection did not occur, and a more accurate distribution of soil moisture availability. The results suggest an optimal approach wherein convection is forced where lightning was observed and totally suppressed in the absence of lightning. The mere forcing of prior convection, however, can help to prevent some spurious triggering of convection in the forecast period. A continental warm-season forecast from an initial condition that included such effects of prior convection showed more skill than a control forecast, at least over a short term. The assimilation scheme implemented in this study ingests lightning data directly, without additional analysis to estimate rainfall per flash as in a prior assimilation scheme. Direct ingest makes the scheme more appropriate for use in a rapid update cycle forecast.

The results suggest that the assimilation is most effective with total lightning data, such as from the ground-based lightning mapping array or data that could be acquired by a satellite-based optical system. Assimilating ground strike data alone does improve the initial condition of the forecast period, but not as much as assimilating total lightning data does. The reason is that, with 10-km model grid spacing, ground strike data alone depict less detail and area of storm structure than total lightning data provide. With larger grid spacing, the difference may not be as great. It may be possible to develop a more sophisticated algorithm for using ground-strike data that would improve the NLDN-only assimilation, perhaps by using an influence radius for each CG flash.

As a byproduct of developing the lightning assimilation technique, it has been qualitatively confirmed that lightning compares rather well with another more traditional proxy for convection, heavy rainfall. Rainfall amounts with and without the assimilation of lightning densities (from NLDN) were compared with a national rainfall mosaic produced routinely by the National Centers for Environmental Prediction (NCEP). The quantitative precipitation estimates during the spin-up cycle of the control run (without assimilation) was roughly 10% of the observed amounts, implying that the integrated precipitation from all activated subgrid convection was significantly under-forecast. Results indicate that the precipitation forecast during the lightning assimilation period was up to about 40% of observed amounts.

This supports the conclusion that forcing subgrid convection by lightning realistically maintains the intensity and coverage of convection and implies that the under-prediction of convective precipitation during the forecast period is due to difficulty in maintaining the cold pool and triggering new convection along the cold pool boundary. The latter difficulty in maintaining forecast storm intensity may be related to the trigger function formulation and the coding approximations of microphysics and hydrometeor advection in the trailing stratiform (resolved-scale) region of the MCSs during the assimilation and forecast periods. Since spatial coverage is rather accurately specified during assimilation, the under-diagnosed precipitation implies either that the subgrid convection scheme inherently under-predicts convective rainfall or that the model environment has a significant dry (precipitable water) bias, or some combination of these two factors. Since precipitation is intimately connected to development and maintenance of both subgrid- and resolved-scale boundary layer cold pools in the assimilation and forecast cycles, a dry bias in rainfall amounts is consistent with accelerated weakening of the forecast MCS in our case study, compared with observations. (The observed MCS actually maintained its intensity for over 6 hours.)

In our assimilation study, it appeared advisable to us to undo some coding simplifications in COAMPS in the implementation of KF and resolved-scale physics, which appear to have been made for computational efficiency. Such efficiencies may degrade the model physics (and forecast) more than is worthwhile for the gain in computational speed. Two examples are the calculation of the quantity eqfrc in the Kain-Fritsch scheme and the deactivation of advection of snow and rain at scales larger than dxmeso (in COAMPS version 3, it appears that cloud ice also is also not advected at these scales). The first example actually causes a decrease in computational efficiency by necessitating the promotion of real variables to double precision. In the second example, the ad hoc filtering of resolved-scale transport and microphysical processes is not physically justifiable and is expected to produce errors in predicted intensity of the non-convective (e.g., trailing stratiform) regions and the boundary layer cold pool, because of the feedback process proceeding from convective detrainment through non-convective regions to force the development of new convection.

CONCLUSIONS

Results of This Study

Analysis of radar data and lightning data for a few storms showed that total lightning flash rates were correlated with graupel mass and updraft volume, as well as being correlated with several measures of storm intensity, particularly with the area of the storm and the estimated hail probability or maximum hail diameter. Numerical simulations of many storms supported the validity of these correlations and also showed that lightning flash rates are correlated with updraft mass flux through the mixed phase region.

The relationship with updraft likely would be very useful for data assimilation to nudge the intensity of convection, as well as the existence and location of convection. The correlation with precipitating ice could also be used, though perhaps not as directly as the correlation with updraft. However, we need to analyze a larger set of storms from more regions to provide a better statistical basis before attempting to assimilate this information.

Assimilating lightning data to control parameterized convection in the spin-up cycle of the COAMPS mesoscale model has been shown to be promising in improving the effects of prior convection on the initial condition of the forecast period. Lightning data were assimilated directly by using the trigger function of the Kain-Fritsch subgrid convective parameterization. Where lightning was observed, moisture was nudged in 0.1 g kg^{-1} increments (to a maximum of 1 g kg^{-1}) until a parcel in the most unstable layer ascended to an altitude $\geq$7 km and achieved an updraft speed of 10 m s^{-1}. Options were added to weaken or eliminate convection in a grid cell if lightning was not observed there. Assimilating lightning data directly (instead of through an estimate of rainfall per flash that has to be calibrated for each day and region in which it is used) makes the assimilation results consistent with the physics of the model, is simpler, and is more suitable for a rapid update cycle forecast.

In a test case from the central United States in July 2000, the initial conditions for the forecast period were compared when spinning up the model with and without assimilation of lightning data. The assimilation greatly improved initial soil moisture, quantitative precipitation estimates, the location and intensity of surface cold pools, and the location of deep convection at the time of forecast initialization. The best results were obtained when convection was completely suppressed where no lightning was observed. Though assimilating ground strike data alone improved the initial condition of the forecast period, the improvement was not as great as from assimilating total lightning

data. The reason is that, with 10-km model grid spacing, ground strike data alone depict less detail and area of storm structure than total lightning data provide. The results from ground strike data alone may be comparable to those from total lightning data when the model grid spacing is substantially larger. It may also be possible to develop a more sophisticated algorithm for using ground-strike data that would improve the ground-strike-only assimilation for a 10-km grid, perhaps by using a radius of influence for each cloud-to-ground flash.

Improving initialization was the main goal of our assimilation, but effects on the forecast also were studied. The location and amounts of model precipitation diverged increasingly from observations during the forecast period, but up to twelve hours later showed some improvement over the forecast based on no assimilation. It appears that the increasing discrepancy with time was caused at least partly by the tendency of COAMPS to produce too little subgrid-scale convective precipitation. Even during the assimilation cycle, the larger rainfall rates were 40% of observed rates, and this decreased to 20% of observed rates in the first hour of the forecast. Similarly, the forecast temperature gradients weakened with time, whereas observed temperature gradients remained strong. Our hypothesis is that the under-production of subgrid-scale rainfall also reduced surface cooling and outflow boundaries, which tended to weaken subsequent triggering of convection; this, in turn, subsequently produced an even greater shortage of subgrid and resolvable scale rainfall in a feedback cycle.

Future Work Needed

Though this project was successful (a) in developing techniques for assimilating total lightning data and (b) in finding relationships between lightning and other storm properties that may be useful for assimilation, several issues remain:

1. To provide a better statistical basis for using lightning relationships with updrafts and graupel to influence the strength and character of convection, it is highly desirable to broaden the analysis of these relationships to many more storm cases.
2. Because the subgrid-scale convective parameterization tended to produce too little precipitation in COAMPS and effects of this appeared to feed back during the forecast period to weaken subsequent convection, it would be helpful to try to increase the precipitation yield so that improvements in the initial condition will extend farther into the forecast period.
3. It should be possible to make further improvements to the intensity and character of convection for the initial condition of the forecast period by developing assimilation techniques that use lightning not only to turn the convective trigger function on or off, but also to influence the strength and character of the convection. Further work also is needed to investigate the situations under which the option to suppress convection in the absence of lightning during assimilation improves the initial condition, as observed in our test case.

Two approaches for using lightning data to constrain the strength or character of convection were suggested by the observational and storm modeling component of the present grant research. However, these approaches have not yet been pursued, because implementation would require substantial time to modify the design and coding of the KF subgrid convective parameterization, and there was not enough support for the additional labor left in the grant after pursuing the more basic approaches. The two approaches are as follows:

1. Constrain the dynamical properties of the convection directly. For example, one could modify the subgrid updraft profile to nudge convection toward certain

morphologies based on lightning rates.

2. Constrain the microphysical character of subgrid convection. This would differ more from the present approach than nudging updrafts. However, it would be possible to use either a simplified cloud model that includes electrification (e.g., Mansell et al. 2005) or a look-up table of relationships derived from both observations and numerical cloud models for different climatological regimes to derive a local bulk precipitation efficiency to control rainfall rate in a modified Kain-Fritsch model.

The present assimilation method is applied on mesoscale grid meshes of order 10 km or larger, so deep moist convection must be represented by a subgrid-scale parameterization. Since forecast models are increasingly trending toward explicit ensemble prediction of convection on gridmeshes of 2 km or less, the present techniques should be adapted to these future high resolution forecast models and should include the geostationary satellite total lightning mapping data planned within ten years. It may be possible to adapt the present assimilation approach to force explicit convection on fine grids by using some combination of "pseudo-dynamic" (e.g., updraft mass flux vs. total lightning rate) and "pseudo-microphysical" (e.g., graupel volume vs. total lightning rate) forcing proportional to the total lightning flash rate as presented in the observational/modeling subsections of this report. Furthermore, it may be possible to adapt the methods developed by this project to nudge future high-spatial-resolution ensemble forecasts to efficiently improve initial conditions of the forecast period for the ensemble.

Educational Activities

This grant provided funding for the Masters Degree of one graduate student and for helping to start the professional career of one postdoctoral scientist in atmospheric sciences. The lightning mapping array purchased with matching funds for this project was one of three key facilities in a recent field program in central Oklahoma which provided five graduate students and twenty-six undergraduate students with experience collecting storm data in a field program. These data currently are the object of research by seven graduate students, three in the Masters Degree programs in meteorology at the University of Oklahoma, one in the Masters Degree program in atmospheric sciences at Texas A&M, and three in the doctoral program in meteorology at the University of Oklahoma. Data from the Oklahoma Lightning Mapping Array also were used for the doctoral research project of one student in physics at New Mexico Institute of Mining and Technology. Other graduate students from the above institutions and from Colorado State University are also likely to use data from the Oklahoma Lightning Mapping Array in their research projects.

REFERENCES

Alberty, R., T. Crum, and F. Toepfer, 1991: The NEXRAD program: past, present, and future; a 1991 perspective. *25th Int. Conf. on Radar Meteorology*, Paris, France, Amer. Meteor., Soc., 1-8.

Alexander, G. D., J. A. Weinman, V. M. Karyampudi, W. S. Olson, and A. C. Lee, 1999: The effect of assimilating rain rates derived from satellites and lightning on the forecasts of the 1993 superstorm. *Mon. Wea. Rev.*, **127**, 1433–1457.

Baker, H. B., H. J. Christian, and J. Latham, 1995: A computational study of the relationships linking lightning frequency and other thundercloud parameters. *Quart. J. Roy. Meteor. Soc.*, **99**, 10627–10632.

Black, R.A., and J. Hallett, 1999: Electrification of the hurricane. *J. Atmos. Sci.*, **56**, 2004–2028.

Boccippio, D. J., K. L. Cummins, H. J. Christian, and S. J. Goodman. 2001: Combined Satellite- and Surface-Based Estimation of the Intracloud–Cloud-to-Ground Lightning Ratio over the Continental United States. *Mon. Wea. Rev.*, **129**, pp. 108–122.

Bringi, V.N., K. Knupp, A. Detwiler, L. Liu, I.J. Caylor, and R. A. Black, 1997: Evolution of a Florida thunderstorm during the Convection and Precipitation/Electrification Experiment: The case of 9 August 1991. *Mon. Wea. Rev.*, **125**, 2131-2160.

Brooks, I. M. and C. P. R. Saunders, 1994: An experimental investigation of the inductive mechanism of thunderstorm electrification. *J. Geophys. Res.*, **99**, 10627–10632.

Carey, L. D. and S. A. Rutledge, 1996: A multiparameter radar case study of the microphysical and kinematic evolution of a lightning producing storm. *J. Meteor. and Atmos. Phys.*, **59**, 33–64.

Carey, L. D. and S. A. Rutledge, 1998: Electrical and multiparameter radar observations of a severe hailstorm. *J. Geophys. Res.*, **103**, 13979–14000.

Carpenter, R. L., K. K. Droegemeier, and A. M. Blyth, 1998: Entrainment and detrainment in numerically simulated cumulus congestus clouds. Part I: General results. *J. Atmos. Sci.*, **55**, 3417–3432.

Chang, D.-E., J. A. Weinman, C. A. Morales, and W. S. Olson, 2001: The effect of spaceborne microwave and ground-based continuous lightning measurements on forecasts of the 1998 Groundhog Day storm. *Mon. Wea. Rev.*, **129**, 1809–1833.

Cummins, K.L., M.J. Murphy, E.A. Bardo, W.L. Hiscox, R.B. Pyle, and A.E. Pifer, 1998: A combined TOA/MDF technology upgrade of the U.S. National Lightning Detection Network. *J. Geophys. Res.*, **103**, 9035-9044.

Dye, J.E., J.J. Jones, W.P. Winn, T.A. Cerni, B. Gardiner, D. Lamb, R.L. Pitter, J. Hallet, and C.P.R. Saunders, 1986: Early electrification and precipitation development in a small isolated Montana cumulonimbus. *J. Geophys. Res.*, **91**, 1231-1247.

Gardiner, B., D. Lamb, R. L. Pitter, J. Hallett, and C. P. R. Saunders, 1985: Measurements of initial potential gradient and particle charges in a montana summer thunderstorm. *J. Geophys. Res.*, **90**, 6079–6086.

Gish, O. H., 1944: Evaluation and interpretation of the columnar resistance of the atmosphere. *Terr. Magn. Atmos. Electr.*, **49**, 159–168.

Goodman, S.J., D.E. Buechler, P.D. Wright, and W.D. Rust, 1988: Lightning and precipitation history of a microburst-producing storm. *Geophys. Res. Lett.*, **15**, 1185-1188.

Hodur, R. M., 1997: The Naval Research Laboratory's coupled ocean/atmosphere mesoscale prediction system (COAMPS). *Mon. Wea. Rev.*, **125**, 1414–1430.

Helsdon, J. H., Jr. and R. D. Farley, 1987: A numerical modeling study of a montana thunderstorm: 2. model results versus observations involving electrical aspects. *J. Geophys. Res.*, **92**, 5661–5675.

Helsdon, J. H., Jr., W. A. Wojcik, and R. D. Farley, 2001: An examination of thunderstorm charging mechanisms using a two-dimensional storm electrification model. *J. Geophys. Res.*, **106**, 1165–1192.

Huo, Z., and B. Fiedler, 1998: The impacts of ADAS cloud analysis on the simulation of a coastal squall line. Annual report to the Coastal Meteorology Research Program, ed. B. Fiedler, School of Meteorology, University of Oklahoma, 177 pp.

Jayaratne, E.R., C.P.R. Saunders, and J. Hallett, 1983: Laboratory studies of the charging of soft hail during ice crystal interactions. *Q. J. Roy. Meteor. Soc.*, **109**, 609-630.

Jayaratne, E. R., 1993: The heat balance of a riming graupel pellet and the charge separation during ice-ice collisions. *J. Atmos. Sci.*, **50**, 3185–3193.

Kain, J. S., 2004: The Kain-Fritsch convective parameterization: An update. *J. Appl. Meteor.*, **43**, 170–181.

Kain, J. S. and J. M. Fritsch, 1993: Convective parameterization for mesoscale models: The Kain–Fritsch scheme, in *The Representation of Cumulus Convection in Numerical Models, Meteor. Monogr., No. 46*, Amer. Meteor. Soc., Boston, 165–170.

Keith, W. D. and C. P. R. Saunders, 1990: Further laboratory studies of the charging of graupel during ice crystal interactions. *Atmos. Res.*, **25**, 445–464.

Klemp, J. B. and R. B. Wilhelmson, 1978: Simulations of right- and left-moving storms produced through storm splitting. *J. Atmos. Sci.*, **35**, 1097–1110.

Krehbiel, P. R., R. J. Thomas, W. Rison, T. Hamlin, J. Harlin, and M. Davis, 2000: GPS-based mapping system reveals lightning inside storms. *EOS, Trans. Amer. Geophys. U.*, **81**, 21-25.

Lang, T., et al., 2004: The Severe Thunderstorm Electrification and Precipitation Study (STEPS). *Bull. Amer. Meteor. Soc.*, **85**, 1107–1125.

Larson, H.R., and E.J. Stansbury, 1974: Association of lightning flashes with precipitation cores extending to height 7 km. *J. Atmos. Terrestrial Phys., 36,* 1547-1553.

Lhermitte, R. and P. R. Krehbiel, 1979: Doppler radar and radio observations of thunderstorms. *IEEE Trans. on Geoscience Electron.*, **GE-17**, 162–171.

Lopez, R.E. and J.P. Aubagnac, 1997: The lightning activity of a hailstorm as a function of changes in its microphysical characteristics inferred from polarimetric radar observations. *J. Geophys. Res.* **102**, 16,799-16,813.

MacGorman, D.R., D.W. Burgess, V. Mazur, W.D. Rust, W.L. Taylor, and B.C. Johnson, 1989: Lightning rates relative to tornadic storm evolution on 22 May 1981. *J. Atmos. Sci.*, **46**, 221-250.

MacGorman, D. R., and W. D. Rust, 1998: *The Electrical Nature of Storms*. Oxford University Press, New York, 422 pp.

MacGorman, D. R., J. M. Straka, and C. L. Ziegler, 2001: A lightning parameterization for numerical cloud models. *J. Appl. Meteor.*, **40**, 459-478.

MacGorman, D. R., W. D. Rust, P. Krehbiel, W. Rison, E. Bruning, and K. Wiens, 2005: The electrical structure of two supercell storms during STEPS. *Mon. Wea. Rev.*, in press.

Mansell, E. R., 2000: *Electrification and lightning in simulated supercell and nonsupercell thunderstorms*. Ph.D. thesis, University of Oklahoma, Norman, OK.

Mansell, E. R., D. MacGorman, C. L. Ziegler, and J. M. Straka, 2002: Simulated three-

dimensional branched lightning in a numerical thunderstorm model. *J. Geophys. Res.*, **107**, doi:10.1029/2000JD000244.

Mansell, E. R., D. R. MacGorman, C. L. Ziegler, and J. M. Straka, 2005: Charge structure in a simulated multicell thunderstorm. *J. Geophys. Res.*, **110**, doi: 10.1029/2004JD005287.

Marshall, C. H., K. C. Crawford, K. E. Mitchell, and D. J. Stensrud, 2003: The impact of the land surface physics in the operational NCEP Eta model on simulating the diurnal cycle: Evaluation and testing using Oklahoma Mesonet data. *Wea. Forecasting*, **18**, 748-768.

Marshall, T.C., Rust, W.D., and Stolzenburg, M., 1995. Electrical structure and updraft speeds in thunderstorms over the southern Great Plains. *J. Geophys. Res.*, **100**, 1001– 1015.

Mitzeva, R. and C. P. R. Saunders, 1990: Thunderstorm charging: Calculations of the effect of ice crystal size and graupel velocity. *J. Atmos. Terr. Phys.*, **52**, 241–245.

Pereira Fo., A. J., K. C. Crawford, and D. J. Stensrud, 1999: Mesoscale precipitation fields. Part II: Hydrometeorologic modeling. *J. Appl. Meteor.*, **38**, 102–125.

Pereyra, R. G., E. E. Avila, N. E. Castellano, and C. Saunders, 2000: A laboratory study of graupel charging. *J. Geophys. Res.*, **105**, 20803–20812.

Petersen, W.A., and S.A. Rutledge, 1998: On the relationship between cloud-to-ground lightning and convective rainfall. *J. Geophys. Res.*, **103**, 14025-14040.

Rison, W., R. J. Thomas, P. R. Krehbiel, T. Hamlin, and J. Harlin, 1999: A GPS-based three dimensional lightning mapping system: Initial observations in New Mexico. *Geophys. Res. Lett.*, **26**, 3573-3576.

Reap, R.M., and D.R. MacGorman, 1989: Cloud-to-ground lightning: Climatological characteristics and relationships to model fields, radar observations, and severe local storms. *Mon. Wea. Rev.*, **117**, 518-535.

Reynolds, S. E., M. Brook, and M. F. Gourley, 1957: Thunderstorm charge separation. *J. Meteor.*, **14**, 426–436.

Rogers, R. F. and J. M. Fritsch, 1996: A general framework for convective trigger functions. *Mon. Wea. Rev.*, **124**, 2438–2452.

Rogers, R. F., J. M. Fritsch, and W. C. Lambert, 2000: A simple technique for using radar data in the dynamic initialization of a mesoscale model. *Mon. Wea. Rev.*, **128**, 2560–2574.

Rust, W. D., and D. R. MacGorman, 2002: Possible inverted-polarity electrical structures in thunderstorms during STEPS. *Geophys. Res. Lett.*, **29**, 1571, doi: 10.1029/2001GL014303.

Rust, W. D., D. R. MacGorman, E. C. Bruning, S. A. Weiss, P. R. Krehbiel, R. J. Thomas, W. Rison, T. Hamlin, and J. Harlin, 2005: Inverted-polarity electrical structures in thunderstorms in the Severe Thunderstorm Electrification and Precipitation Study (STEPS). *Atmos. Res.*, **76**, doi: 10.1016/j.atmosres.2004.11.029, 247–271.

Saunders, C. P. R. and S. L. Peck, 1998: Laboratory studies of the influence of the rime accretion rate on charge transfer during crystal/graupel collisions. *J. Geophys. Res.*, **103**, 13949–13956.

Saunders, C.P.R., S.L. Peck, G.G. Aguirre Varela, E.E. Avila, and N.E. Castellano, 2001: A laboratory study of the influence of water vapour and mixing on the charge transfer process during collisions between ice crystals and graupel. *Atmos. Res.*, **58**, 187-203.

Solomon, R. and M. Baker, 1998: Lightning flash rate and type in convective storms. *J. Geophys. Res.*, **103**, 14079–14096.

Stensrud, D.J., 1996: Effects of persistent, midlatitude mesoscale regions of convection on the large-scale environment during the warm season. *J. Atmos. Sci.*, **53**, 3503-3527.

Stensrud, D.J., and J.-W. Bao, 1992: Behaviors of variational and nudging assimilation techniques with a chaotic low-order model. *Mon. Wea. Rev.*, **120**, 3016-3028.

Stensrud, D.J., and J.M. Fritsch, 1994a: Mesoscale convective systems in weakly forced large-scale environments. Part II: Generation of a mesoscale initial condition. *Mon. Wea. Rev.*, **122**, 2068-2083.

Stensrud, D.J., and J.M. Fritsch, 1994b: Mesoscale convective systems in weakly forced large-scale environments. Part III: Numerical simulations and implications for operational forecasting. *Mon. Wea. Rev.*, **122**, 2084-2104.

Storm Data, 2000: available from the NOAA National Climatic Data Center, 151 Patton Ave., Asheville, NC 28801-5001 or from www.ncdc.noaa.gov.

Straka, J. M., 1989: *Hail Growth in a Highly Glaciated Central High Plains Multi-cellular Hailstorm*. Ph.D. thesis, University of Wisconsin-Madison, Dept. of Meteorology, Madison, WI 53706.

Straka, J. M. and E. R. Mansell, 2005: A bulk microphysics parameterization with multiple ice precipitation categories. *J. Appl. Meteor.*, **44**, 445-466.

Takahashi, T., 1978: Riming electrification as a charge generation mechanism in thunderstorms. *J. Atmos. Sci.*, **35**, 1536-1548.

Takahashi, T., 1983: Numerical simulation of winter cumulus electrification. Part I: Shallow cloud. *J. Atmos. Sci.*, **40**, 1257–1280.

Takahashi, T., 1984: Thunderstorm electrification – a numerical study. *J. Atmos. Sci.*, **41**, 2541–2558.

Tessendorf, S. A., and S. A. Rutledge, 2002: Kinematic and microphysical evolution of the 29 June supercell during STEPS. *Preprints, 21st Conf. on Severe Local Storms*, Amer. Meteor. Soc., San Antonio, TX, 307–310.

Thomas, R. J., P. R. Krehbiel, W. Rison, T. Hamlin, D. J. Boccippio, S. J. Goodman, and H. J. Christian, 2000: Comparison of ground-based 3-dimensional lightning mapping observations with satellite-based LIS observations in Oklahoma. *Geophys. Res. Lett., 27*(12), 1703-1706, 10.1029/1999GL010845.

Thomas, R., P. Krehbiel, W. Rison, S. Hunyady, W. Winn, T. Hamlin, and J. Harlin, 2004: Accuracy of the lightning mapping array. *J. Geophys. Res.*, **109**, D14207, doi: 10.1029/2004JD004549.

WATADS (WSR-88D Algorithm Testing and Display System) 2000: Reference Guide for Version 10.2 [Available from Storm Scale Applications Division, National Severe Storms Laboratory, 1313 Halley Circle, Norman, OK 73069.]

Watson, A.I., R.L. Holle, R.E. López, and R. Ortiz, 1991: Surface wind convergence as a short-term predictor of cloud-to-ground lightning at Kennedy Space Center. *Wea. and Forecasting, 6*, 49-64.

Weisman, M. L. and J. B. Klemp, 1982: The dependence of numerically simulated convective storms on vertical wind shear and buoyancy. *Mon. Wea. Rev.*, **110**, 504–520.

Wiens, K. C., S. A. Tessendorf, and S. A. Rutledge, 2003: STEPS June 29, 2000 Supercell: Observations of kinematic, microphysical, and electrical structure. *Proceedings, 12th Int. Conf. on Atmospheric Electricity*, ICAE, Versailles, France, 263–266.

Wilks, D.S., 1995: Statistical methods in the atmospheric sciences, an introduction. Academic Press, 467 pp.

Williams, E.R., M.E. Weber, and R.E. Orville, 1989: The relationship between lightning type and convective state of thunderclouds. *J. Geophys. Res.*, **94**, 13,213-13,220.

Williams, E., B. Boldi, A. Matlin, M. Weber, S. Hodanish, D. Sharp, S. Goodman, R. Raghavan, and D. Buechler, 1999: The behavior of total lightning activity in severe Florida thunderstorms. *Atmos. Res.*, **51**, 245-265.

Williams, E. R., 2001: The electrification of severe storms, Severe Convective Storms. *Meteor. Monogr.*, C. A. Doswell, III, ed., Amer. Meteor. Soc., volume 50, 527–561.

Wojcik, W. A., 1994: *An Examination of Thunderstorm Charging Mechanisms Using the IAS 2D Storm Electrification Model.* Master's thesis, So. Dakota Schl. Mines Technol., Rapid City, SD.

Ziegler, C., 1999: Issues in forecasting Mesoscale Convective Systems: An observational and modeling perspective, in Vol. 2, Chapter 32, *Storms*, R. Pielke, Jr. and R. Pielke, Sr, Eds., Routledge Press, London, 26-42.

Ziegler, C. L., P. S. Ray, and D. R. MacGorman, 1986: Relations of kinematics, microphysics and electrification in an isolated mountain thunderstorm. *J. Atmos. Sci.*, **43**, 2098–2114.

Ziegler, C. L., D. R. MacGorman, J. E. Dye, and P. S. Ray, 1991: A model evaluation of noninductive graupel-ice charging in the early electrification of a mountain thunderstorm. *J. Geophys. Res.*, **96**, 12833–12855.

Ziegler, C. L. and D. R. MacGorman, 1994: Observed lightning morphology relative to modeled space charge and electric field distributions in a tornadic storm. *J. Atmos. Sci.*, **51**, 833–851.

Ziegler, C. L., W. J. Martin, R. A. Pielke, Sr., and R. L. Walko, 1995: A modeling study of the dryline. *J. Atmos. Sci.*, **52**, 263-285.

Ziegler, C. L., T. J. Lee, and R. A. Pielke, Sr., 1997: Convective initiation at the dryline: A modeling study. *Mon. Wea. Rev.*, **125**, 1001-1026.